Molecular Systems Design & Engineering

REVIEW

Elastin-Like Polypeptides as Building Motifs toward Designing Functional Nanobiomaterials

Received 00th January 20xx,
Accepted 00th January 20xx

DOI: 10.1039/x0xx00000x

www.rsc.org/

Duc H. T. Le[a, b] and Ayae Sugawara-Narutaki*[c]

Taking inspiration from naturally-occurring proteins, scientists have created protein polymers consisting of functional amino acid sequences that have evolved in nature. The functions of protein polymers can be custom-designed through the modular assembly of protein domains or minimized functional motifs. Elastin-like polypeptides (ELPs) are one of the exquisite building motifs in designing protein polymers. They exhibit stimuli-responsive self-assembling properties, remarkable elasticity, and favorable biological characteristics such as low platelets adhesion and low immunogenicity. With these characteristics, ELP-based materials have been demonstrated to be promising candidates for nanobiomaterial applications such as tissue engineering, drug delivery, and nanobiodevices. This review describes the recent developments in designing modular protein polymers containing ELPs as the building units.

1. Introduction

Proteins are the ultimate functional molecules comprising various modular structural or functional units, defined as protein domains. Significant developments in protein engineering have provided in-depth understanding of the protein sequence–structure–function relationships and have thus stimulated intense interest from material scientists in creating artificial protein polymers mimicking the known protein domains that have evolved in nature.[1-3] For example, repetitive structural motifs or minimized functional motifs in proteins are typically used as building units in custom-designed protein polymers, either singularly or combined, for new functional materials.[4-6] These ingenious polymers, with their applications in the bio- and nanotechnology fields, have become an essential part in the current state-of-the-art material designs.

Functional motifs in elastin, a self-assembling protein that provides biological tissues with elasticity and resilience, are one of the key building blocks in designing protein polymers.[7-9] Elastin is an essential extracellular matrix (ECM) proteins that is abundantly found in blood vessels, lungs, ligaments, and skin. At these connective tissues, the protein organizes into networks of elastic fibers which are capable of supporting indefinite cycles of stress and relaxation.[10-12] Mature elastin is formed after the self-assembly and crosslinking of the precursor protein, tropoelastin. Despite its unique mechanical and self-assembling properties, the adaptation of naturally occurring elastin in biomaterials has been underexplored because its intrinsic insolubility makes elastin manipulation relatively challenging.[13,14] Therefore, researchers attempted to "dissect" the elastin molecule (i.e., tropoelastin) to determine the key sequences that are responsible for its remarkable elasticity and/or self-assembly. In 1974, Urry *et al.* had a breakthrough in this attempt and revealed that a polypentapeptide (Valine-Proline-Glycine-Valine-Glycine)$_n$ (VPGVG)$_n$, which mimics one of the repeating sequences found in tropoelastin, could undergo a reversible phase separation identical to that in the native molecule in an aqueous solution.[15] The phenomenon is known as coacervation process in polymer science, and is temperature-responsive. Following this finding, Urry's group conducted thorough research on the physicochemical and biological properties of (VPGVG)$_n$ and its derivatives.[16] In addition, Tamburro *et al.* independently reported the unique self-assembling properties of fragments "dissected" from tropoelastin using the reductionist approach.[17-20] Based on their systematic studies, a myriad of functional protein polymers containing elastin-derived sequences have been constructed along with rapid progress in synthetic chemistry and genetic engineering.[7-9] These protein polymers are typically called elastin-like polypeptides (ELPs). Given that ELPs could have inherited the self-assembling and remarkable mechanical properties from tropoelastin, more and more researchers have joined the field. This review focuses on the recent developments in the design strategies of modular protein polymers containing ELPs as the building units. We begin by describing characteristic sequences found in tropoelastin and then discuss the progress in designing ELPs with tandem repeats of tropoelastin-derived sequences. Finally, we provide various examples of ELP-based block copolymers, in which different types of ELPs are connected in one molecule, or in which ELPs are fused to other proteins. These modular macromolecules

[a] Department of Biomedical Engineering, Eindhoven University of Technology, P.O. Box 513 (STO 3.25), 5600MB Eindhoven, The Netherlands
[b] Department of Biochemistry, Radboudumc, Geert Grooteplein 28, 6525 GA Nijmegen, The Netherlands
[c] Department of Materials Chemistry, Graduate School of Engineering, Nagoya University, B2-3(611) Furo-cho, Chikusa-ku, Nagoya 464-8603, Japan. E-mail: ayae@chembio.nagoya-u.ac.jp

This journal is © The Royal Society of Chemistry 20xx

Please do not adjust margins

have attracted great attention because of the controllability and engineerability of self-assembled structures, stimuli-responsive properties, mechanical properties, and biocompatibility. Protein purification by conjugating ELP to a protein of interest is also one crucial application; however, we have not included this topic here because excellent reviews can be found elsewhere.[21]

2. Domains and Motifs in Elastin

Tropoelastin, the precursor protein of elastin, is a 72-kDa molecule comprising highly repetitive amino acid sequences. The domain structure of tropoelastin is shown in Fig. 1.[22] There are three kinds of domains: proline-rich hydrophobic, glycine-rich hydrophobic, and crosslinking domains. The crosslinking domains are rich in lysine (K) residues and thus relatively hydrophilic. Mature elastin is stabilized by crosslinking between primary amines in K residues to form desmosine or isodesmosine structures through lysyl oxidase. On the other hand, the hydrophobic domains of tropoelastin are essential for its self-assembly processes.[17-20] The proline-rich hydrophobic domains contain abundant amount of P, V, G, and alanine (A) residues and are found within the middle region in tropoelastin. Tamburro *et al.* have shown that some proline-rich domains, such as exons 18, 20, and 24, behave similarly to tropoelastin when isolated.[17] They undergo a reversible, temperature-induced coacervation through dehydration and rehydration of the hydrophobic side chains. On the other hand, termini-located glycine-rich hydrophobic domains share consensus repeating motif XGGZG (X, Z: V or L). Interestingly, exons 28, 30, and 32 also show temperature-dependent dehydration, but irreversibly assemble to form amyloid-like fibers.[18,20,23] Keeley *et al.* hypothesized that the glycine-rich hydrophobic domains play an important role in determining the mechanical properties of elastin because of their intrinsic tendency to form β-sheets to produce rigid structures.[24] In another work, the C-terminal glycine-rich exons were hypothesized to be critical for the elastin fiber self-assembly.[25]

Tropoelastin also contains a bioactive peptide motif GRKRK at exon 36. The sequence allows an integrin $\alpha_v\beta_3$ binding for cell adhesion.[26] Weiss *et al.* were the first group to succeed in expressing a full-length human tropoelastin, and have since developed tropoelastin-based biomaterials and examined their biological activities for tissue engineering applciations.[27,28] In addition to the tropoelastin-based materials, ELP protein polymers based on the essential tandems found in tropoelastin (i.e., the proline- and glycine-rich hydrophobic domains) also play important roles in the elastin-based material field, which is the main subject of this review.

3. Design rationales for repeating motifs in ELPs

3-1. ELP sequences inspired from the proline-rich domains

ELPs inspired from the proline-rich hydrophobic domains are the most common designs in the field. The ELP sequences are generally tandems of a pentapeptide subunit (VPGXG) (X: any amino acid except P),[16] although other uncommon subunits were also reported.[29,30] This simple repeating sequence $(VPGXG)_n$ shows self-assembly behavior, the so-called coacervation, that is subject to temperature changes, similar to that in tropoelastin.[16,31] Each ELP has a defined lower critical solution temperature (LCST) or transition temperature (T_t). At below T_t, ELPs exist in extended random-coiled structures; the hydrophobic side chains are hydrated by ordered water molecules, making the proteins soluble in aqueous solvents. By increasing the solution temperature, ELPs transform from coils to β-spiral structures consisting of consecutive type II β-turns (Fig. 2a–c), and at the same time, they expel the bound water, leading to exposure of hydrophobic side chains.[32, 33] Here, P at the second and G at the third position

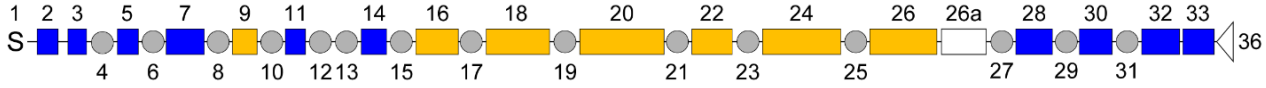

Domain name	Exon number	Peptide sequnce
Proline-rich hydrophobic domain	18	GAAAGLVPGGPGFGPGVVGVPGAGVPGVGVPGAGIPVVPGAGIPGAAVP
	20	GARPGVGVGGIPTYGVGAGGFPGFGVGVGGIPGVAGVPSVGGVPGVGGVPGVGIS
	24	ALLNLAGLVPGVGVAPGVGVAPGVGVAPGVGLAPGVGVAPGVGVAPGVGVAPGI
Glycine-rich hydrophobic domain	28	GAAVPGVLGGLGALGGVGIPGGVV
	30	GLVGAAGLGGLGVGGLGVPGVGGLG
	32	GAAGLGGVLGGAGQFPLG
Crosslinking domain	8	GAVVPQPGAGVKPGKVP
	25	GPGGVAAAAKSAAKVAAKAQL

Fig. 1 Domain structure encoded by human tropoelastin gene and the peptide sequences of several representative exons from each domain.[22] S stands for the signal sequence. Human tropoelastin lacks exons 34 and 35.

This journal is © The Royal Society of Chemistry 20xx

Please do not adjust margins

are crucial to β-turn formation (Fig. 2a and 2b).[33] After dehydration, the hydrophobic ELP tends to aggregate via hydrophobic interaction to form particulate structures. The process is favorable in terms of thermodynamics because the increase in ordered ELPs (i.e., decrease in entropy) can be compensated by the decrease in ordered water (i.e., increase in entropy). It should be noted that molecular dynamics simulations have indicated that the described β-spiral is too "ideal" for ELPs; $(VPGXG)_n$ were recently shown as predominantly random coil polymers in which each repeat is independently capable of transiently sampling β-turn and polyproline type II (PPII) structure.[34,35]

The responses of ELPs toward thermal triggers are quite sharp, occurring within 1-2 °C; hence, this property is utilized extensively for developing stimuli-responsive materials.[36,37] Various strategies can be applied to precisely manipulate T_t. First, hydrophobicity and mean polarity are the parameters that affect T_t greatly.[38,39] The higher the hydrophobicity, the lower the T_t. This can be tuned by increasing the lengths or repeat numbers (n) of ELPs, or by replacing the X position in $(VPGXG)_n$ with more hydrophobic amino acids. Phenylalanine (F), tyrosine (Y), and/or isoleucine (I) are typically introduced to enhance overall hydrophobicity for lowering T_t.[16,40] On the other hand, the substitution of less hydrophobic and more neutral residues, such as A, could raise T_t;[39,41] the effect of which would be more pronounced with charged residues, such as K or glutamic acid (E).[42] Also, it is not limited in using a single guest residue to adjust the mean polarity and hydrophobicity. Multiple guest residues can be well-mixed throughout the polymer chain to precisely control T_t of the whole sequence.[41] For example, a hydrophilic $(VPGXG)_n$ uses the alternatives of guest residues A, G, or V distributed at a ratio of 8:7:1, respectively, with the resultant T_t significantly higher than 37 °C. Second, the ionic strength of solvents, which can be adjusted by salt addition, is another method to manipulate T_t.[43] ELPs were shown to have lower T_t in solvents containing anions categorized as kosmotropes. These anions are highly hydrated and thus influence the water shield on ELPs. Anions categorized as chaotropes, which have lower hydration degrees, would increase T_t if the anions are at low concentrations. At high concentrations, the effects of chaotropic anions are reversed, which would decrease T_t because of the dominant hydration on the anions than on the ELPs. Reagents, such as sodium dodecyl sulfate and urea, disrupt the hydrogen bonds in the β-turns and prevent the polypeptides from forming ordered structures.[16,44] As a result, T_t of ELPs would increase in the presence of these reagents. Trifluoroethanol (TFE), on the other hand, enhances hydrophobic interaction and hydrogen bond formation, thus it promotes the secondary structural transition, and self-assembly along with the decrease in T_t.[45] Finally, T_t is also influenced by ELP concentrations —a higher ELP concentration will result in a lower T_t.[38] By following these general observations, several computational models have been developed (Fig. 2d).[41,46,47] They allow for the prediction of T_ts of ELPs with precision fit and thus reduce the number of trials and errors. In addition to the thermoresponsive properties, ELPs that are responsive to additional stimuli, such as pH, light, and ion concentrations were also constructed.[48-50]

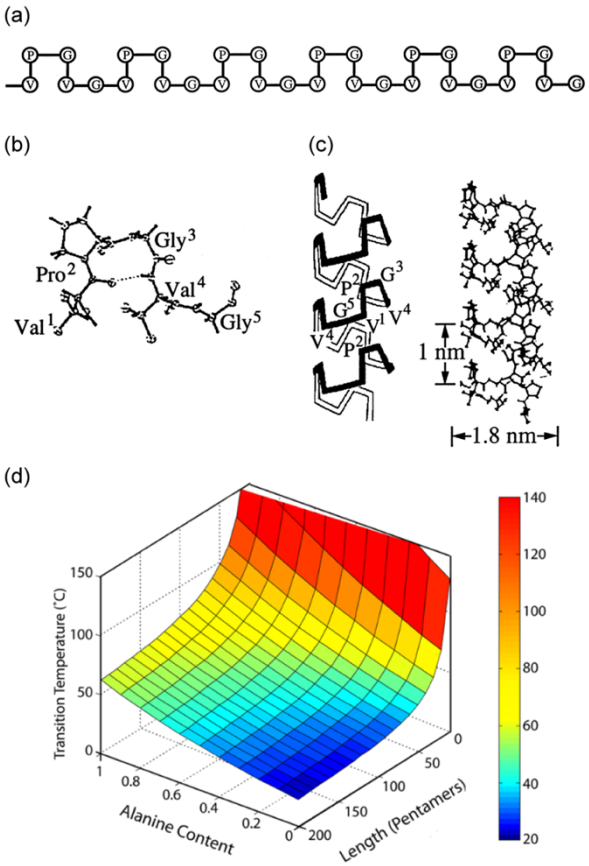

Fig. 2 (a-c) Molecular structure of the β-spiral consisting of consecutive β-turns from the polypentapeptide $(VPGVG)_n$. Schematic of the repetitive β-turns (a), formed by proline (P) at the second position and glycine (G) at the third position in a pentapeptide subunit (b). (c) Helical representations of β-spiral structures adopted by $(VPGVG)_n$ showing the turn position within each turn of the helix (left) and the detailed plots in stereo-pair view showing the helical pitch (1 nm) and the diameter of the spiral structure (1.8 nm) (right). Reproduced and adapted with permission from ref. 33. Copyright 1997, American Chemical Society. (d) A three-dimensional plot showing the relationship between the substitution content of the guest residue, here alanine (A), and the lengths of $(VPGXG)_n$ vs transition temperatures. Reproduced and adapted with permission from ref. 41. Copyright 2013, American Chemical Society.

Please do not adjust margins

Using reversible stimuli-response by thermal triggers, ELPs have found a myriad of applications, including using ELP-based nanoparticles as carriers for loading and delivering drugs. For example, a $(VPGXG)_{160}$ (X: V, A, or G) was fused to a C-terminal sequence containing eight cysteines $(GGC)_8$ for conjugation with drug (here is Doxorubicin, DOX) via a maleimide–thiol coupling reaction.[51] The conjugated ELP–DOX molecule, which have an amphiphilic structure consisting of the hydrophilic ELP (T_t >> 37 °C) and the hydrophobic drug domain, spontaneously assembles into micellar structures with an ELP corona (Fig. 3a). In fact, hydrophilic ELP was shown to enhance plasma circulation and might also facilitate tumor homing and accumulation.[52] Mice treated with the ELP–DOX have shown a four-fold higher maximum tolerated dosage because of the drug encapsulation.[51] After a single injection, a significant decrease in tumor volume was observed, implying the high efficacy of ELP–DOX treatment.[51] In another work by Huang *et al.*, an ELP designated 40 repeating subunits comprising guest residues V and histidine (H) at the ratio 1:4 was fused with the tumor necrosis factor-related apoptosis-inducing ligand (TRAIL).[53] The ELP-based nanoparticles were constructed by heating to 37 °C. In this case, the ELP coacervated to form the hydrophobic core while TRAIL is displayed on the nanoparticle surface for cell–nanoparticle interaction (Fig. 3b). Despite some reports on these formulates, $(VPGXG)_n$-based nanoparticle systems usually lack precise control of their sizes or stabilities. To expand the use of ELPs in drug delivery, block copolymers from multiple ELP domains are more beneficial. This will be reviewed in the next section.

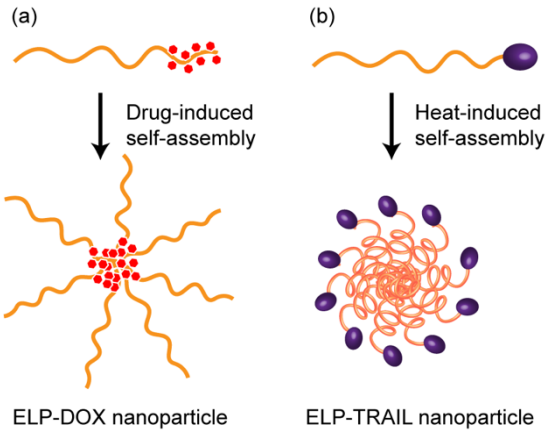

Fig. 3 Schematic of $(VPGXG)_n$-based nanoparticle models. (a) High molecular weight of ELP with a C-terminal domain containing C residues for DOX conjugation. The presence of the hydrophobic DOX and the hydrophilic ELP enables the formation of micelles with a core packed with DOX and a hydrophilic ELP corona. (b) ELP was genetically fused with TRAIL; the nanoparticle is formed by self-assembly of the ELP domain and presents multivalent TRAIL proteins on its surface.

3-2. Hydrogels from $(VPGXG)_n$-based ELPs

Proline-rich domain-inspired ELPs are attractive sources for preparing hydrogels for use as artificial scaffolds in tissue engineering. The use of ELP-based hydrogels has several advantages. (1) $(VPGXG)_n$-based ELPs can be synthesized with high yield (up to subgram scale per litre culture), high purities and excellent monodispersities, due to the optimized production from bacterial systems. (2) ELPs can be precisely custom-designed by genetic engineering; therefore, (3) ELP-based hydrogels can be precisely controlled over structures and functions. (4) Finally, ELP-based materials are biocompatible, biodegradable, and non-immunogenic. We will discuss several approaches to functionalize ELP-based hydrogels applicable for tissue engineering.

Hydrogels can be formed by coacervation of $(VPGXG)_n$ at temperatures above its T_t. Typically, ELPs require relatively high repeat numbers, such as $(VPGXG)_{90}$ (X: V, G, A at a ratio 5:3:2, respectively) or $[VGRGD(VGVPG)_6]_{20}$ (RGD is for cell adhesion).[54,55] To stabilize ELP hydrogels, physical or chemical crosslinking was conducted. Physical crosslinking utilizes relatively weak forces, such as hydrophobic interaction, electrostatic interaction, and hydrogen bonds. These forces can be introduced by adding various sequences, such as silk-like sequences, which will be discussed in the following sections. Leucine zippers are another option to create stable and reversible hydrogels;[56] however, the focus on chemical crosslinking has been more dominant, given that a wide variety of ELPs containing different crosslinkable groups have been produced and examined with various crosslinkers. One simple strategy is to replace the X position with a K residue to provide crosslinkable amino groups. Crosslinkers with different crosslinking activity and with different levels of biocompatibility were examined; some of these were glutaraldehyde, bis(sulfosuccinimidyl) suberate, β-[tris(hydroxymethyl)phosphino]propionic acid, genipin, and pyrroloquinoline quinone.[57] Depending on the degree of crosslinking and the number of K residues in ELPs, the mechanical properties of hydrogels can be manipulated within a range of 1–1000 kPa.[57] Although these approaches are relatively fast and efficient, chemical crosslinking has some drawbacks such as difficulty in achieving homogenous crosslinking, the use of organic solvent, and potential toxicity of the crosslinkers. These drawbacks should be carefully considered especially when one prepare *in situ* cell-encapsulating scaffolds.

To overcome these pitfalls, transglutaminase-catalyzed crosslinking between ELPs carrying glutamine (Q) or K residues provided an alternative in which the reaction could take place under mild conditions (Fig. 4a).[58,59] For this purpose, ELPs with 112 repeats, in which 17 guest positions were replaced by 16 Q and 1 K residues, denoted as [QV6-112], or replaced by 17 K residues, denoted as [KV6-112], were constructed.[58] These

 This journal is © The Royal Society of Chemistry 20xx

Please do not adjust margins

guest residues with amino groups are susceptible to the enzyme-catalyzed reaction (Fig. 4a). The crosslinked ELP hydrogels encapsulating chondrocytes showed an increase in dynamic shear moduli from 0.28 to 1.7 kPa over 4 weeks of culture. The formation of cartilage matrix was confirmed *in vitro* with the presence of type II, but not type I collagen, which suggested hyaline cartilage formation. De Torre *et al.* have described another rapid, yet biocompatible method using catalyst-free "click" chemistry. Here, ELPs containing K residues were first modified to obtain two separate ELPs functionalized with two different reactive groups—one carrying azides and the other carrying an activated alkyne group (here, cyclooctyne).[60] Mixture of these functionalized ELPs in water at 20 °C rapidly formed hydrogels via the click chemistry reaction (Fig. 4b). This strategy homogenously encapsulated various cell types including human primary fibroblasts (HFF1), human primary umbilical vein endothelial cells (HUVEC), and human adipose-derived tissue mesenchymal stem cells (MSC) and thus could be beneficial for preparing injectable hydrogels or *in situ* drug delivery depots.[60,61] Glassman *et al.* have described a crosslinking approach using redox reaction via cysteines (C).[62] The ELP was designed as 50 repeats of $[(I^{0.6}V^{0.4})PAVG]$ flanked by two cell-adhesive sequences containing C residues at the two termini.[62] The rationale behind this design was that an ELP chain could be further extended by disulfide bond formation (Fig. 4c), resulting in an extensible, tough hydrogel with Young's moduli ranging from 5 kPa to 1 MPa depending on the ELP concentration (5–30%). Furthermore, the networks were shown to resist ~~to~~ erosion over long-term incubation in water at 37 °C. More stable and extensible ELP gels can be created by further crosslinking through ELP backbones in the presence of photoinitiators (Irgacure® 2959) (Fig. 4c).[63] The resulting gel is highly extensible, with up to a 420% strain. *In vitro* and *in vivo* studies have indicated long-term structural stability and no immune responses during early and progressive host integration.

Finally, for constructing bioactive ELP hydrogels, functional sequences that promote cell binding and proliferation are essential because $(VPGXG)_n$ is bioinert toward cells. RGD is typically used but other sequences, such as those from laminin, type IV collagen, and native elastin itself, were also examined.[64] Recently, an ELP containing RGD for general cell adhesion; REDV for specific endothelial cell adhesion; and a bioactive $(VGVAPG)_n$, which is sensitive to elastase, was constructed.[65] The hydrogel from this ELP can support blood vessel infiltration in addition to the controllable degradability from VGVAPG, while the control samples without the corresponding sequence blocked infiltration and prevented host cell invasion in the *in vivo* vascularization model.[65] So far, functionalized ELP-based hydrogels have been tested *in vitro* and *in vivo* for cartilage repair, liver tissue engineering, cardiovascular applications, wound healing, and ocular tissue engineering and their potentials applications are expanding. Details on various applications are available in several reviews.[57,66,67]

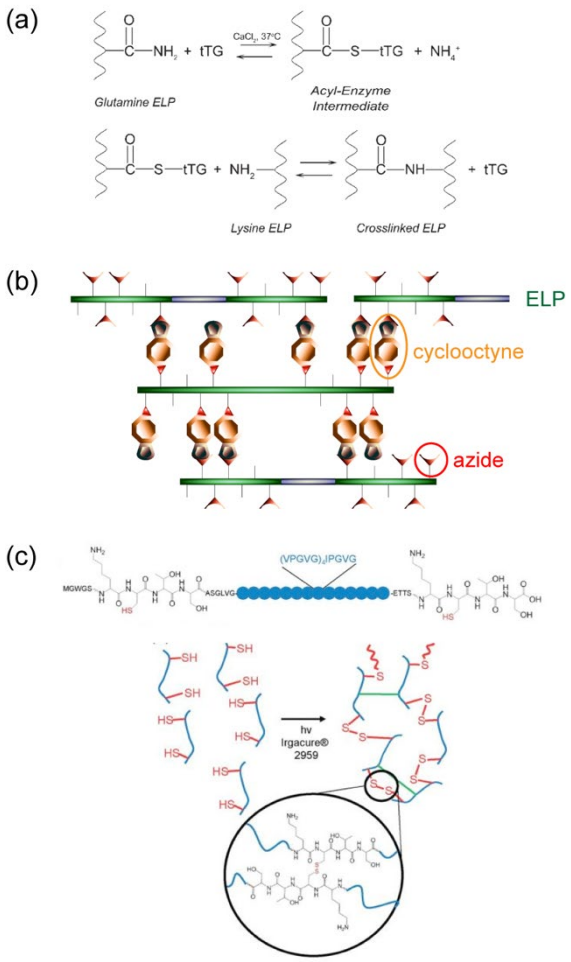

Fig. 4 Various biocompatible crosslinking strategies for preparing ELP hydrogels. (a) The reaction scheme for transglutaminase-catalyzed crosslinking between Q or K side chains in ELPs. Reproduced and adapted with permission from ref. 58. Copyright 2005, Mary Ann Liebert, Inc. (b) Catalyst-free "click" chemistry between ELPs carrying azide and ELPs carrying cyclooctyne results in immediate formation of ELP gels that can encapsulate cells *in situ*. Reproduced and adapted with permission from ref. 60. Copyright 2014, Elsevier. (c) The sequence of ELP with two crosslinking sites containing C side chains appended at the two termini for ELP extension as well as crosslinking (red line). Treatment by UV irradiation in the presence of the photoinitiators results in further crosslinking between the ELP backbones (green line). Reproduced and adapted with permission from ref. 63. Copyright 2015, Wiley-VCH.

3-3. ELP sequences inspired from the glycine-rich domains and their amyloid formation

Despite not being as appealing as its counterpart $(VPGXG)_n$, another series of ELP designs should be considered because they exhibit distinct self-assembly properties. Here, ELPs with a repeating subunit described as XGGZG, in which X and Z are either V or L, were chemically synthesized. Poly(VGGVG), poly(VGGLG), and poly(LGGVG) were first synthesized using polycondensation reactions; it should be noted that these poly(XGGZG)s have quite broad degrees of polymerization (DP) with average values from 5–7. They were used for side-by-side

Please do not adjust margins

comparison to elucidate factors that influence self-assemblies.[68-70] For example, the work comparing poly(VGGVG) and poly(LGGVG) revealed that, with only one additional -CH_2- in leucine (L) at the first position, these polypeptides showed distinct assembled morphologies.[71] The deposit of a poly(VGGVG) suspension, after prolonged incubation in water at ambient temperature (20 °C), consisted of well-defined fibers with bead-on-string morphologies as shown in the atomic force microscopy (AFM) images (Fig. 5a and 5b). Circular dichroism (CD) and Fourier-transform infrared (FT-IR) spectra confirmed the formation of predominant β-sheet structures immediately after preparation of poly(VGGVG) suspension; the secondary structures changed slightly at various temperatures (0 °C, 25 °C, and 70 °C). Congo Red assay confirmed that these fibers have amyloid-like features indicated by the red shift of the absorbance spectrum from 495 to 503 nm. On the other hand, poly(LGGVG) formed dendritic-like structures (Fig. 5c) together with networks of short, entangled fibrils from globular assemblies (Fig. 5d). The polypeptide showed the presence of β-turns together with unordered conformation. In the follow-up work, the effects of solvents including methanol (MeOH), ethylene glycol (EG), dimethylsulfoxide, and water, were investigated given that each would impart different degrees of solvation and an intrinsic propensity to aggregate (i.e., hydrogen bond formation).[72] Again, poly(VGGVG) assembled best into networks of fibers in water, but fibrous morphologies were also observed in MeOH and EG. Interestingly, adding MeOH gave rise to the formation of amyloid-like structures for poly(LGGVG), which is in agreement to the reported effects of alcohol-based solvents on inducing amyloid fiber formation.[73] However, the broad distribution of the DPs in poly(XGGZG) appeared to be a factor that greatly influenced ~~to~~ self-assembled structures. Using solid-phase peptide synthesis methods, homogenous $(VGGVG)_3$, $(LGGVG)_3$, $(VGGLG)_3$, and $(LGGLG)_3$ were constructed.[74,75] The obtained assemblies contrasted with the observed corresponding poly(XGGZG) counterparts. While $(VGGVG)_3$ can also form β-sheet structures, entangled and short fibrils but not elongated fibers were detected (Fig. 5e).[74,75] On the other hand, the fibril-forming propensity of $(LGGVG)_3$ was higher than that of $(VGGVG)_3$, which was reflected by bundles of twisted fibrils with a maximum length of approximately several micrometers (Fig. 5f).[75] In $(LGGLG)_3$, short straight fibrils (< 1 μm) that associated into flocks were observed (Fig. 5g).[75] $(VGGLG)_3$ formed straight nanorods rather than fibrils (Fig. 5h). The position of V and L in the pentapeptide (XGGZG) appeared to be an important factor determining which nanostructure formed. These works have provided some general rules for designing fiber-forming ELPs using the basic XGGZG sequence. To move toward to tissue engineering applications, functionalization and the corresponding evaluation are needed. The first evaluation indicated that at least these (XGGZG)-type amyloid-like fibers are biocompatible with the tested cells, such as fibroblasts and human mesenchymal stem cells.[74,76] Boraldi *et al.* have shown that heparan sulfates can be used to facilitate these ELPs to form harmless amyloid fibers with high biocompatibility.[77]

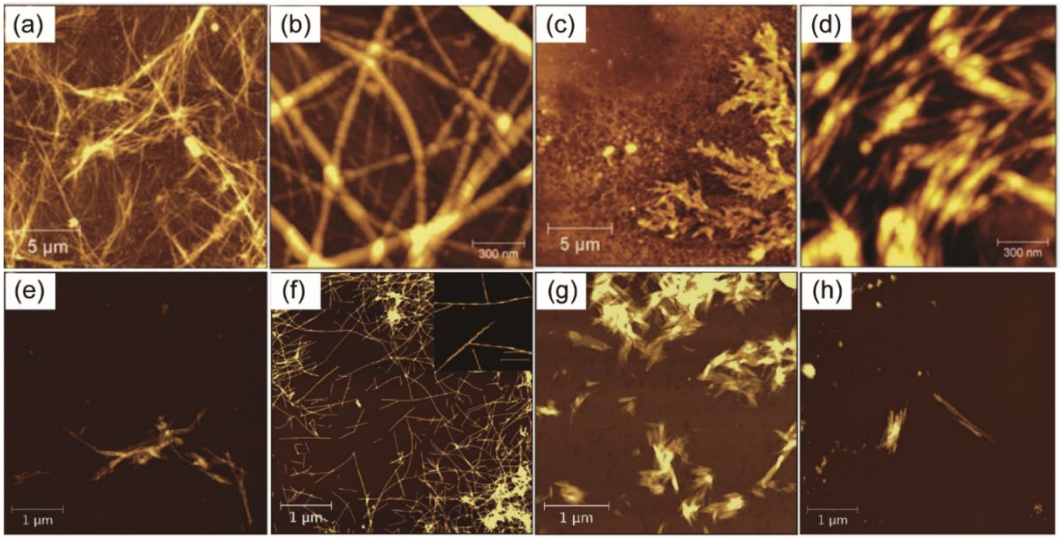

Fig. 5 AFM images of the assembled structures from $(XGGZG)_n$-based ELPs. (a, b) Amyloid-like fibers assembled from poly(VGGVG). (c) Dendritic-like morphologies and (d) short fibrils from globular assemblies of poly(LGGVG). Reproduced and adapted with permission from ref. 71. Copyright 2011, Wiley Periodicals, Inc. (e-h) Assembled structures of $(VGGVG)_3$ (e), $(LGGVG)_3$ (f), $(LGGLG)_3$ (g), and $(VGGLG)_3$ (h). Reproduced and adapted with permission from ref. 75. Copyright 2015, Royal Society of Chemistry.

This journal is © The Royal Society of Chemistry 20xx

Please do not adjust margins

4. ELP block copolymer design rationales

Advances in genetic engineering allow *de novo* designs and synthesis of tailor-made block copolymers from different ELP motifs with exquisite control over sequence lengths, compositions, and arrangements.[78-81] For example, the cloning technique described as recursive directional ligation by plasmid reconstruction (Pre-RDL), developed by Chilkoti *et al.*, is advantageous not only in constructing ELP clones that have high repeat numbers but also in combining multiple ELP genes and/or functional domains seamlessly in a predetermined order.[80] By elaborating two or more blocks exhibiting different properties (e.g., hydrophobicity vs. hydrophilicity, polar vs. nonpolar nature, and secondary structures), it is possible to obtain a myriad of block copolymer designs, in which their self-assemblies result in intriguing nanomorphologies ranging from micelles, vesicles, fibrils, nanofibers, to hydrogels, implying the versatility and usefulness of ELP-based building blocks for nanobiomaterials. In addition, libraries of ELP block copolymers were constructed, providing an understanding of the design parameters to precisely tune the structures-functions as desired. These ELP assembled nanostructures have useful applications in drug delivery and tissue engineering as proof-of-concept and some have been tested in both preclinical and clinical trials. In this section, we divide ELP block copolymer designs based on their specific assembled structures including nanoparticles, nanofibers, and hydrogels.

4-1. ELP block copolymer forming nanoparticles

To obtain nanoparticles, ELP block copolymers can be designed as diblock amphiphiles in which a hydrophilic ELP block is conjugated with a hydrophobic ELP block (Fig. 6). Here, the term “hydrophobicity” or “hydrophilicity” is determined by a relative comparison between the two block components. One with a lower transition temperature T_t is defined as the hydrophobic ELP, and the other with higher T_t is defined as the hydrophilic one. With an amphiphilic block structure, micelles can be obtained via self-assembly upon thermal triggers (Fig. 6). At a temperature below both T_ts, a diblock ELP remains a soluble unimer while being solvated by water molecules. At an elevated temperature range between the lower and higher T_t, the hydrophobic block is selectively dehydrated and thus aggregates to form the dense hydrophobic core, while the hydrophilic block remains solvated and exposed to solvents, forming the corona of the formed micelles. Further increasing the temperature results in the dehydration of the hydrophilic block, leading to aggregation of micelles into sub-micron particles. The temperatures at the transition from unimers to micelles and from micelles to aggregates are defined as critical micelle temperature (CMT) and aggregation temperature ($T_{aggregation}$), respectively. By rationally selecting appropriate ELP sequences, micelle properties including CMTs, diameters, and aggregation numbers (ELP chains per one particle) can be finely tuned.

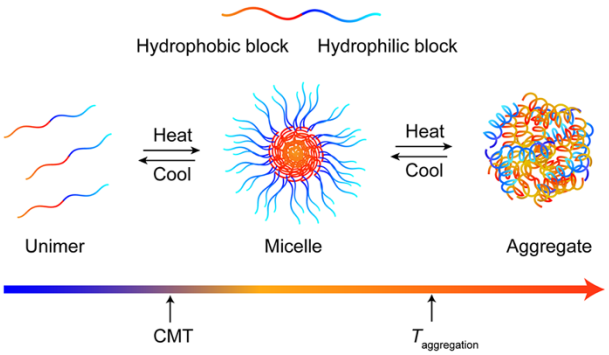

Fig. 6 Schematic of an amphiphilic block ELP assembling into nanoparticles upon thermal triggers. The amphiphilic ELP contains a hydrophobic block with a lower T_t and a hydrophilic block with a higher T_t. At temperatures above the CMT, micelles are formed by the association of the hydrophobic block while the hydrophilic block forms the micelle corona. Heating to temperatures higher than $T_{aggregation}$, the block ELP becomes completely hydrophobic and thus polydisperse micro-sized aggregates are formed. Cooling reverses the process, in which the aggregate disassembles to return to the unimer form.

An example of the amphiphilic model is the combination of a charged hydrophilic $[VPGEG(IPGAG)_4]_{14}$ block and a hydrophobic $[VPGFG(IPGAG)_4]_{16}$ block, first developed by Conticello *et al.*[82] The rationales behind this block design are that the presence of the guest residues (i.e., E and F residues) would maximize the difference between hydrophilicity and hydrophobicity by polarity between the two blocks, and the hydrophobic block sequence alone would self-assemble at ambient temperatures. In addition, the introduction of the charged residues in the hydrophilic block would facilitate charge-dipole interactions of the hydrophilic side chains and solvents, thus ensuring micelle dispersity. The system showed temperature- and pH-dependent self-assemblies. At 40 °C, which is significantly higher than the lower T_t of the hydrophobic block, presence of monodisperse micelles with diameters of 87 ± 15 nm were confirmed by dynamic light scattering (DLS). Noteworthy, at 25 °C in a neutral solvent (water), the assembled structures of the diblock ELP observed by transmission electron microscopy (TEM) were both spherical and beaded filaments with diameters of 59 ± 9 and 50 ± 10 nm, respectively. This suggested that the elongated structure was the result of coalescence among the spherical aggregates. Under basic conditions, monodisperse particles with a narrow distribution were observed, which most likely resulted from the increase in charge repulsion from E residues. In another design, concentration-dependent self-assembly of a diblock ELP designated as $[(VPGVG)_2(VPGEG)(VPGVG)_2]_{50}$-$(VPGIG)_{60}$ was observed.[83] At 1 mg.mL^{-1}, the diblock ELP formed micellar structures, as seen in Fig. 7a. The diameters of the micelles increased with the increase in concentration up to 8 mg.mL^{-1} as determined by DLS. After increasing the concentrations to 10 mg.mL^{-1}, two different morphologies—spherical and cylindrical

Please do not adjust margins

—were observed (Fig. 7b). The diameter of the micelles appeared to be smaller than the diameter of those assembled at the lower concentrations. It is hypothesized that the micelle reached critical size and lost its stability as a result of repulsion from the charged block, creating a smaller stable micelle. On the other hand, the cylindrical morphologies might be the result of the association between the hydrophobic cores by hydrophobic interaction. With a further increase in the concentration to 50 $mg.mL^{-1}$, hydrogel clusters made of one-dimensional association of micelles were detected (Fig. 7c). At 100 $mg.mL^{-1}$, lyotropic hydrogel was formed; small-angle X-ray scattering (SAXS) and scanning electron microscopy (SEM) confirmed the hexagonal structures within the fibril forming a hydrogel (Fig. 7d). The hypothesis of this morphological transition is illustrated in Fig. 7e. These works imply the ability to engineer of ELP-based diblock copolymers for tunable nanostructures.

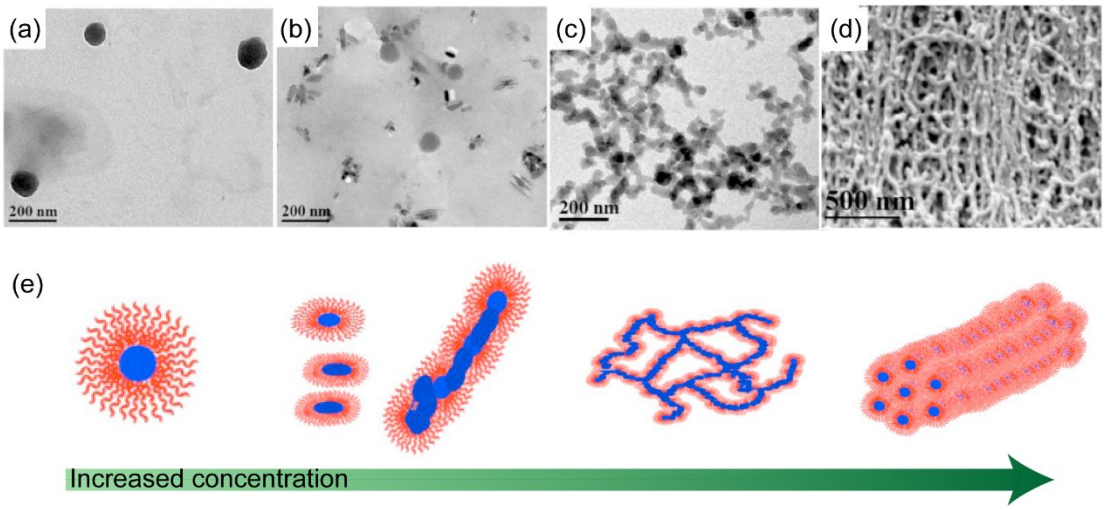

Fig. 7 (a-d) Morphologies of the assembled structures from $[(VPGVG)_2(VPGEG)(VPGVG)_2]_{50}$-$(VPGIG)_{60}$ as a function of concentration in water. TEM images of nanoparticles at 1 $mg.mL^{-1}$ (a), cylindrical and spherical morphologies mixture at 10 $mg.mL^{-1}$ (b), cryoEM image of hydrogel clusters at 50 $mg.mL^{-1}$ (c), and SEM image of the fibrillar structure at 100 $mg.mL^{-1}$ (d). (e) Schematic of the morphological transition in a concentration-dependent manner. Reproduced and adapted with permission from ref. 83. Copyright 2015, Elsevier.

Chikoti *et al.* have constructed a library of amphiphilic diblock ELPs based on the sequence $[VPGVG(VPGGG)_7(VPGAG)_8]_n$-$(VPGVG)_m$ (n: 64, 96, and 128; m: 60, 90, and 120).[80,81,84] DLS, static light scattering (SLS), and cryoEM were used to systematically investigate the effects from the design parameters on self-assembly. A general rule can be made from the experimental observation as follows: ELP block copolymers with a hydrophilic-to-hydrophobic block ratio in between 1:2 and 2:1 are most likely able to form monodisperse micelles. Besides this range, subtle differences in T_ts from the two block components are not sufficient. As a result, diblock ELPs behave as a unimer; therefore, only a unimer-to-aggregate transition is observed. CMTs are tunable by adjusting the length of the hydrophobic block, which determines the corresponding lower range of T_t from the diblock. Micelle diameters are dependent on the relative hydrophilic-to-hydrophobic block length ratios and also the absolute lengths. With these types of ELP sequences, the assembled micelles were defined as "weak" micelles,[85] in contrast to the "strong" micelles assembled from synthetic polystyrene–polyisoprene block copolymers. ELP "weak" micelles were described as having a dense hydrophobic core from the hydrophobic block, while the hydrophilic block stays in a somewhat collapsed state, but not as extended as that in "strong" micelles (Fig. 8). Various theoretical states of the ELP micelles based on surface tensions at the core–corona interface are shown in Fig. 8. The mathematical formulae for predicting CMTs and aggregation numbers for these "weak" micelles have been developed and examined experimentally, showing consistency between the predicted and observed data. These formulae are especially beneficial for constructing ELP-based micelles applicable under the physiological conditions.

An alternative to the above design was to use the hydrophobic block $[(VPGVG)(VPGHG)_4]_m$ instead of $(VPGVG)_m$ to further introduce pH-sensitive and Zn^{2+} ion-sensitive properties.[50] Histidine (H), at pH < 6.4, becomes increasingly protonated; therefore, the assembly from the H-contained block is not favorable because of electrostatic repulsion. It was observed that the diblock ELP behaved like a unimer and only the unimer-to-aggregate phenomenon was observed. Higher pHs, on the other hand, significantly reduced the charges at the H side chain. As a result, the designated ELP became more hydrophobic and the overall T_t of $[(VPGVG)(VPGHG)_4]_m$ decreased. The range between the two T_ts from the hydrophilic and hydrophobic blocks expanded, leading to micelle formation by combining thermal and pH stimuli. The addition of Zn^{2+} ions, which have high affinity toward H residues via coordination, provided the hydrophobic core with physical crosslinking to stabilize the micelles. Decreasing pH conversely resulted in the disassembly. The described diblock ELP could be a useful design for releasing cargo drugs at the disease sites using pH differences in the tumor environment vs. that under normal physiological conditions.

 This journal is © The Royal Society of Chemistry 20xx

Please do not adjust margins

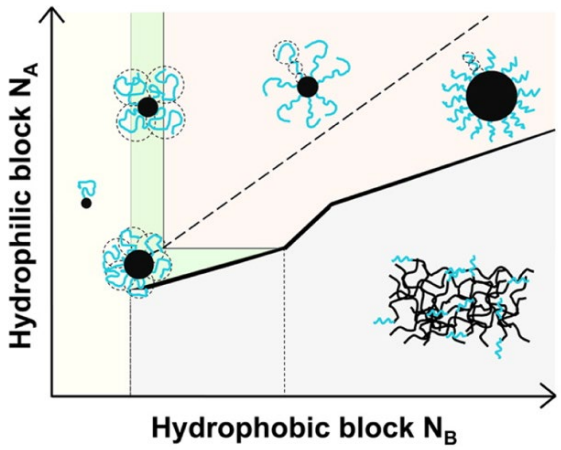

Fig. 8 Diagram illustrating various types of ELP micelles depending on the repeat numbers of the hydrophilic block N_A vs. the repeat numbers of the hydrophobic block N_B. The yellow area depicts where a diblock ELP stays as a unimer. The green area is where "weak" micelles are formed. The pink area is the area of "strong" micelles. The remaining area indicates non-spherical aggregate. Reproduced and adapted with permission from ref. 85. Copyright 2015, American Chemical Society.

Triblock ELPs were also constructed. Sallach *et al.* have developed a triblock sequence with a hydrophilic $[(VPGVG)_2(VPGEG)(VPGVG)_2]_{48}$ block, flanked by the terminal hydrophobic $[(IPAVG)_4VPAVG]_{16}$ blocks, of which T_t is around 20 °C.[86] A pyrene-based fluorescent probe was used to determine micelle formation. Interestingly, the micelles formed at both below and above the T_t of the hydrophobic block; however, CD and FT-IR spectra indicated that there was a secondary structural shift from helices to sheets upon heating. Along with this transition, the micellar core expelled more water molecules and became compact, which was reflected by a size reduction from 122 to 88 nm. This work provided a design strategy for the formation of ELP-based nanoparticles at a wider temperature range, while the materials were still sensitive to a temperature trigger. The reversed block arrangement, where hydrophobic $(VPGAG)_{40}$ was flanked by two hydrophilic $[(VPGVG)_2VPGEG(VPGVG)_2]_{10}$, led to vesicle formation (Fig. 9).[87] This was supported by TEM (Fig. 9b), in which a hollow sphere and a stained wall, typically characterized as vesicles, could be observed. Moreover, the sizes of these nanoparticles can be tuned by adding NaCl.[87] It should be noted that vesicle formation is relatively rare in self-assembling ELPs while it could be useful for high loading capacity for both hydrophobic and hydrophilic drugs.

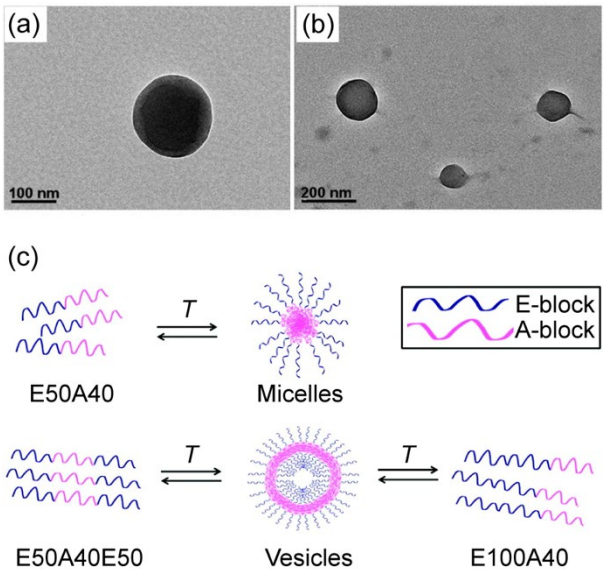

Fig. 9 (a, b) TEM images of the self-assembled structures from diblock E50A40 (a) and triblock E50A40E50 (b). The E-block is based on the monomer $[(VPGVG)_2(VPGEG)(VPGVG)_2]$, whereas the A-block is based on (VPAVG). The numbers indicate the amount of total pentamers in each block. Depending on the block arrangement, micelles (a) and vesicles with hollow structures (b) can be observed. (c) Schematic representation of micelles and vesicles obtained from different diblock and triblock ELPs. Reproduced and adapted with permission from ref. 87. Copyright 2012, American Chemical Society.

Together with fundamental self-assembly studies, ELP-based nanoparticles were further functionalized and evaluated for their potential drug delivery applications. They have been shown to be biocompatible, biodegradable, and non-immunogenic.[29,88,89] The advantages of ELP-based nanoparticles/micelles are that they can be finely tuned to form appropriate sizes (i.e., from 10–100 nm) with excellent monodispersity. Nanoparticles within this size range are advantageous because they can escape renal clearance. Furthermore, enhanced permeability and retention (EPR) effects, the unique phenomenon in the tumor environment where nanoparticles selectively accumulate more than in normal tissues, are facilitated at these particle sizes.[90] The following describes a rational scenario for developing functional ELPs for use in drug delivery. Temperature-sensitive properties of ELPs can be used to form micelles and can concurrently encapsulate therapeutic molecules within their hydrophobic cores. Dipyridamole, an anti-inflammatory drug, and rapamycin, an anticancer agent, have been demonstrated as examples of encapsulated hydrophobic drugs. The resultant solubility was enhanced up to 60–70 times, allowing *in vivo* delivery for inhibiting adhesion of neutrophils to vascular endothelium.[91-93] Meanwhile, one end of the hydrophilic block exposed to solvents can be modified with functional moieties for nanoparticle–cell interactions. These range from small modifiers, such as photosensitizers or fluorescent probes, to macromolecules, such as targeting peptides or protein

Please do not adjust margins

domains.[94] While small molecules could be easily conjugated by conventional chemical reactions, macromolecules are particularly beneficial from genetic cloning for protein-based drug delivery. ELP micelles are useful platforms for the multivalent presentation of targeting ligands to enhance their localization at the disease sites. Various targeting peptide/proteins including IL-4 receptor targeting peptide,[95] fibrinogen binding peptide,[96] and CD13 receptor targeting NGR peptide,[97] have been incorporated into ELP micelles. It is important to note that fusion with relatively large polypeptides/proteins, such as the llama VHH domain or the adenovirus serotype 5 fiber protein, did not alter the micelle-forming ability of ELPs[94,98]; however, this might not apply to all proteins and thus optimization of the ELP constructs might be needed. To enhance the tumor uptake, a cell-penetrating peptide was also elaborated.[99]

Nanoparticle stability is also important and must be controlled. Chemical crosslinking within micelles is a reasonable strategy,[91,92] in addition to the aforementioned methods of tuning hydrophobic lengths or adding ions. To this end, crosslinkable sequences containing K or C were introduced in between the hydrophobic and hydrophilic blocks or at one end of diblock ELPs.[91,92] Disulfide bonds between C residues can be broken by reducing agents, such as tris(2-carboxyethyl)phosphine,[91] while a hydrazone-based linker is sensitive to the pH of the environment,[51] allowing controlled release of cargos.

ELP-based nanomedicine has been showed promising results in suppressing tumor growth *in vivo*, and some have been tested in clinical trials. The potential of ELP-based nanoparticles can be further expanded to have multiple functions. A combination of the engineering approaches described above (i.e., modification and functionalization at both the corona and core to carry more functional moieties) is expected to induce synergetic effects. Meanwhile, when introducing a new function, an appropriate balance must be carefully considered to control particle stability.

4-2. ELP block copolymer forming nanofibers

ELP-based nanofibers are of interest in tissue engineering applications because they mimic the fibrous morphologies of the biological ECM. Le *et al.* have constructed a double-hydrophobic block ELP named "GPG" that self-assembles into nanofibers at the physiological temperature (Fig. 10).[100-104] GPG contains a basic self-assembling sequence $(VGGVG)_5$-$(VPGXG)_{25}$-$(VGGVG)_5$, where X is V(80%) or F(20%). Both the glycine-rich $(VGGVG)_5$ and proline-rich $(VPGXG)_{25}$ dehydrate at the stimulating temperature but each forms a distinct secondary structure, β-sheets and β-turns, respectively. This block design was inspired from the uneven distribution of the glycine-rich and proline-rich hydrophobic domains in tropoelastin. Proline-rich domains localize at the center while glycine-rich domains localize at both ends of the tropoelastin molecule (Fig. 1). In water at above 37 °C, GPG (20 μM) initially assembles into nanoparticles rich in β-turns, followed by the connection into beaded nanofibers along with the formation of β-sheet structures between nanoparticles (Fig. 10b-d).[100,101] It takes ~1 week for GPG to form mature nanofibers in water. The self-assembly of GPG is accelerated in the presence of TFE, which enhances hydrogen bond formation.[102] Nanofibers were formed within 1 h in 30%(v/v) TFE aqueous solution. Unlike amyloid fibrils, GPG nanofibers exhibit a tortuous morphology, and no red shift in the spectrum was observed for Congo Red in the presence of GPG nanofibers.[102] By fusing functional peptide motifs to the C-terminus of GPG, various functionalized nanofibers were obtained. These include thermally-stable crosslinked nanofibers[103] and those with antibacterial[104] or cell-binding[101] properties. The excellent colloidal stability of these nanofibers in water makes them easy-to-handle materials especially for coating or blending.

4-3. ELP block copolymer hydrogels

ELP block copolymers were also designed with a triblock structure for preparing physically crosslinked hydrogels. The ELP comprises a hydrophilic $[(VPGVG)_2(VPGEG)(VPGVG)_2]_{30}$ middle block flanked by two hydrophobic $[(IPAVG)_4(VPAVG)]_{16}$ terminal blocks.[9,105-107] The middle block contains charged residue E to ensure that T_t is significantly above the physiological temperature (~75 °C). Meanwhile, T_t of the terminal block is chosen at the ambient temperature (~20 °C). Therefore, the hydrophobic end blocks act as virtual crosslinking points via thermally reversible hydrophobic association.[105] On the other hand, the middle block remained solvated and behaved like an elastomersimilar to that of native elastin. This triblock ELP has been shown to have robust viscoelastic and mechanical responses ranging from plastic to elastic depending on the block design. For example, the mechanical properties could be tuned by either changing the length of the middle block or amino acid compositions, or by designing twice of the length of the hydrophobic blocks.[106,107] Noteworthy, these physically crosslinked hydrogels based on the triblock ELP have been shown to have long-term biostability up to 1 year *in vivo* and exceptional biocompatibility for use as implanted material.[108]

This journal is © The Royal Society of Chemistry 20xx

Please do not adjust margins

Please do not adjust margins

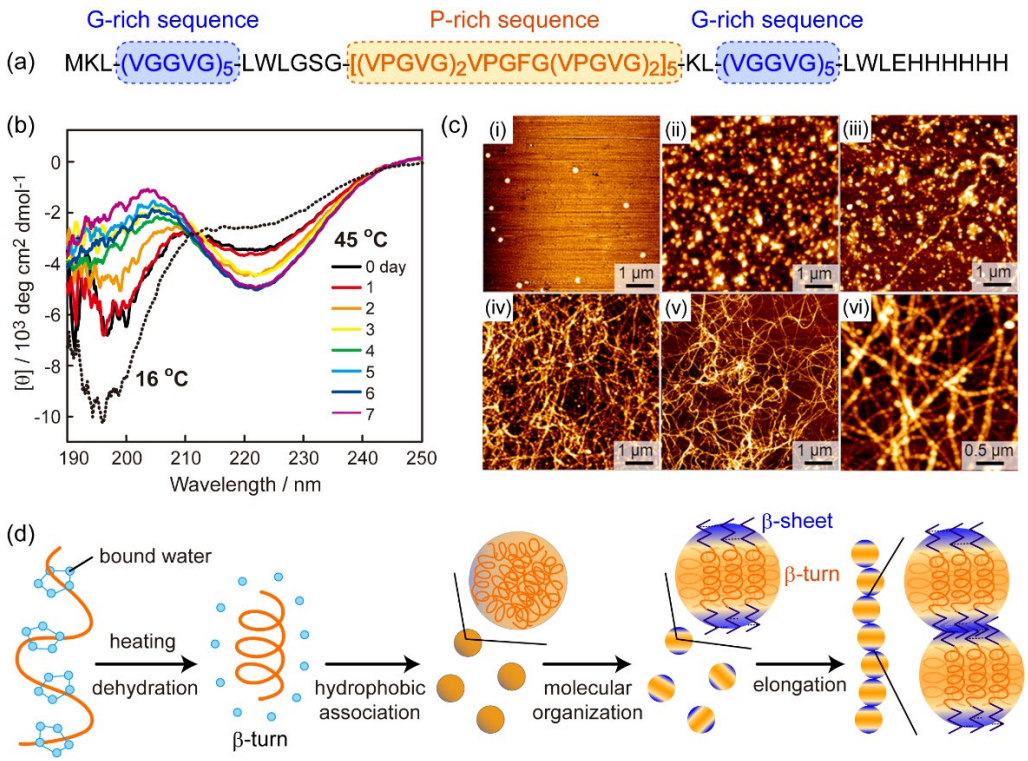

Fig. 10 (a) Amino acid sequence of GPG. (b) Temperature-dependent CD spectra of GPG. (c) AFM images of the assembled structures of GPG formed at 45 °C. (i) Particles formed just after preparation, (ii) particles and (iii) fibers formed after 1 day at different locations on the mica substrate, (iv) fibers formed after 2 days and (v) 7 days, and (vi) the high magnification image of nanofibers with the beaded structure after 7 days. (d) Tentative model for the assembly of GPG into nanofibers. Reproduced and adapted with permission from ref. 100. Copyright 2013, American Chemical Society.

5. Hybrid ELP block copolymer design rationales

In addition to the block copolymers comprising two or more ELPs, hybrid designs, in which an ELP block is combined with another self-assembling block, have also been reported. More elaborate stimuli-responsive systems can be constructed by using self-assembling properties from each block component. The conjugation partner includes silk-like polypeptides, collagen-like polypeptides, resilin-like polypeptides, coiled-coils, or viral coat proteins. Apparently, ELP hybrid systems with synthetic polymers are also possible strategies. Interesting examples could be found in ELP conjugates with poly(ethylene glycol), in which control of the assembled structures was described in detail.[109,110] Very recently, lipid–ELP conjugates were also constructed using post-translational modification methods.[111,112] Fatty acid[111] and cholesterol[112] were incorporated at the N- and C-termini of an ELP, respectively, and the effects of the conjugation on self-assembly were systematically studied; however, this review focuses on protein-based models.

5-1. Silk-elastin-like polypeptides (SELPs)

Silk-elastin-like polypeptides (SELPs) are one of the most intriguing hybrid polypeptides that have been extensively developed and examined for their applications in drug delivery and tissue engineering. Silk-like polypeptides are the biomimetic sequences with a repeating motif $(GAGAGS)_n$ inspired from the natural *Bombyx mori* silk heavy chain.[113,114] The polypeptides tend to form tightly packed β-sheets,[115,116] and thus they can be processed into materials with high tensile strengths.[117,118] Incorporating the soluble ELP domain provides several benefits, such as increased overall solubility of SELPs, because silk-like polypeptides alone are typically hydrophobic and easy to aggregate. The conjugation allows for the convenient fabrication of SELPs in water-based solvents. In addition, if done at appropriate ratios, combining rigid β-sheet-rich silk-like sequences with flexible elastin-like sequences could be used to engineer the mechanical properties derived from the high tensile strength and the excellent resilience from each block component. SELPs are typically designed as multiple repeats of the basic unit $[(GAGAGS)_n\text{-}(VPGXG)_m]$. The self-assembly of SELPs, driven by either the silk block or both block components, results in various nanostructures including nanoparticles, nanofibers, nanogels, and hydrogels. Similar to ELPs, replacing the X positions in the elastin-like block could address new dynamic stimuli-responsive functions from pH, ionic strength, redox, enzymatic stimuli, and electric field. Wang *et al.* developed a combinatorial library approach with high throughput screening to select SELPs with the desired stimuli-responsive functions mentioned above, in conjunction with tensile strength and adhesion.[119] They efficiently selected 64 SELPs with the desired functions from 2,000 recombinant *Escherichia coli* (*E. coli*) colonies for characterization, enabling systematic understanding of sequence-function relationships within this SELP library.

Please do not adjust margins

Please do not adjust margins

Xia *et al.* constructed a series of SELPs named SE8Y, S2E8Y, and S4E8Y. These SELPs have similar molecular weights but are designed with various ratios of the silk-to-elastin blocks in a monomer repeat (Fig. 11a).[120] All of these SELPs formed micellar particles at the ambient temperature by the collapse of the hydrophobic silk-like block. The propensity of micelle formation increased with higher proportions of the silk-like domain. DLS indicated that SE8Y existed as both monomers and micelles, whereas S4E8Y assembled into uniform particles. Increasing the temperature to 60 °C led to the collapse of the ELP block, which induced the formation of various higher ordered structures including larger nanoparticles for SE8Y and S2E8Y and hydrogels for S4E8Y (Fig. 11b). Cooling these suspensions to 20 °C decreased the size of SE8Y particles, while a mix of morphologies including nanofibers was observed for S2E8Y and S4E8Y (Fig. 11b).

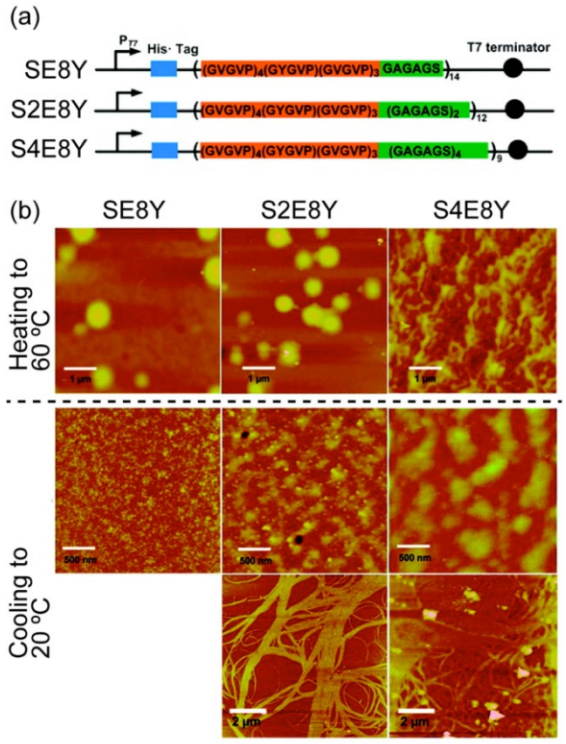

Fig. 11 (a) Schematic of the SELP block structures containing elastin-like blocks (orange) and silk-like blocks (green). The numbers next to each block name (S or E) indicate the numbers of repeats of silk or elastin domain within the brackets. (b) Various self-assembled structures of SE8Y, S2E8Y, and S4E8Y upon heating to 60 °C and after cooling to 20 °C. Reproduced and adapted with permission from ref. 120. Copyright 2011, American Chemical Society.

Although there was a relationship between the silk-to-elastin block ratios and the self-assembly behavior, the mechanism by which the final morphologies were formed remains unclear. In the follow-up work from the same group, the self-assembly of these SELPs could also triggered to form micelles by the introduction of hydrophobic drugs (DOX).[121] Here, the drugs were encapsulated within the hydrophobic core made of the silk-like blocks with the loading yields at 4–6.5 wt%. Drug-loaded SELP nanoparticles were internalized into HeLa cells and delivered DOX into nuclei. The nanoparticle showed a delivery pathway different from that of the free drugs and also showed enhanced toxicity to the cancer cells *in vitro*, suggesting an efficient delivery method, particularly for drug-resistant cancer cell models.

SELPs were also shown to form stable nanogels when they contained a high number of the silk-like blocks, which act as the physical crosslinking points.[122] At above a critical concentration, nanogels were formed and stabilized by β-sheet structures from the silk-like blocks. Nanogel formation was confirmed by a spectroscopic assay using 1-anilinonaphthalene-8-sulfonic acid (1,8-ANS, a hydrophobic fluorescent molecule) as well as SEM. Dilution did not cause the nanogels to break, in contrast to the SELP-based micellar counterparts.[122] Of course, with the presence of ELP, the sizes of the nanogel changed in response to changes in temperatures. The nanogels might be advantageous in high drug-loading capacity than micellar systems.

In addition to forming nanoparticles, SELPs can also assemble into nanofibers. Golinska *et al.* constructed SELPs named S24E40 $((GAGAGE)_{24}$-$[(VPGVG)_5(VPGAG)_3(VPGGG)_2]_4)$ and S12C4E40, in which a random coil spacer, C4, was introduced.[123] Both of these SELPs self-assemble into nanofibrils upon pH stimuli, attributed to the β-sheet-forming silk block. The nanofibrils become sticky and interact with each other with increasing temperatures due to the presence of the elastin-like block. S12C4E40 can further form weak hydrogels at a concentration > 40 wt%. Another report indicated that a specific type of SELPs can form nanofibers on a silicon surface but not in a bulk solution.[124] The silicon substrate assisted nucleation for fiber growth.

The ability to form hydrogels is one of the important features of SELPs that fueled the exploration into tissue engineering. SELPs named 47K, 415K, and 815K were synthesized and their gelation properties were investigated.[125,126] The first number (4 or 8) and the second number (7 or 15) indicate the repeat numbers of the silk-like block and elastin-like block, respectively. K represents one additional elastin repeating unit that has a lysine as the guest residue. Herein, as previously mentioned, silk domains act as physical crosslinking points through the formation of β-sheet structures. When increasing the temperature from 25 °C to 37 °C, at least 4 wt% of the SELP solution was needed for gelation. The hydrogels from these constructed SELPs were characterized to elucidate influences of factors such as block sequences, concentrations, cure time, and ionic strength toward thier swelling and mechanical properties.[126] The crosslinking densities increased with increased silk-to-elastin ratios (i.e., 47K > 815K > 415K). Storage moduli or stiffness determined by dynamic mechanical analysis and the correlation length obtained by small-angle neutron scattering suggested that the length of the ELP block determines the spacing ~~of~~ between crosslink points, while the silk blocks are responsible for stiffness and structural rigidity.

The encapsulation of various cargos, such as naked DNA and virus vectors, has been demonstrated for cancer gene

 This journal is © The Royal Society of Chemistry 20xx

Please do not adjust margins

Please do not adjust margins

therapy.[127,128] The cargo release is influenced by the geometry of the hydrogels and can be controlled by the number of crosslinking points, which also depends on the number of the silk-like blocks as well as the gelation concentrations. Hydrogel degradation can also be manipulated by adding the matrix-metalloproteinases (MMP)-responsive sequence.[129]

Another system of hydrogel-forming SELP was designated as $[(VPGVG)_2VPGEG(VPGVG)_2]_{10}(VGIPG)_{60}$-$[V(GAGAGS)_5G]_2$.[130] The noteworthy points in this design are that the silk-to-elastin block ratio is relatively low, and that the elastin block is designed as an amphiphilic structure. The SELP underwent a two-step assembly. The initial step was based on the reversible self-association of the hydrophobic $(VPIPG)_n$ block to form a soft gel ($G' = 2.5 \times 10^3$ Pa) composed of bridged micelles. The second step was achieved by annealing further at 37 °C to yield the harder gel ($G' = 1 \times 10^4$ Pa) because of the condensation of silk-blocks. Subsequently, the nanostructures matured into fibrillar structures via the arrangement of the β-sheets. These gels are stable and could be used as injectable hydrogels.

5-2. Collagen-elastin-like polypeptides and resilin-elastin-like polypeptides

Collagen is the most abundant protein in mammals and accounts for 25–35% of total protein in humans. *In vivo*, collagen assembles into fibrous structures that constitute a great proportion of nearly all connective tissues.[131] These collagen fibers comprise three PPII-type helices twisted together in a right-handed pattern. These helices are stabilized by hydrogen bonds between the glycine amide in one chain and the carbonyl of the amino acid of an adjacent chain.[132] The biocompatibility, biodegradability, self-assembling abilities, and bioactivities of the protein inspired material scientists to construct a new class of biomimetic polymers called collagen-like polypeptides (CLPs). While the initial intention for preparing CLPs was to elucidate the folding process in native collagens, recent research has shifted the focus to bring CLPs into the biomaterials section.[133-136] Kiick *et al.* have integrated a CLP with a thermo-responsive ELP to create a new self-assembly system.[137] The collagen-like counterpart, designated as $(GPO)_4GFOGER(GPO)_4GG$, and the ELP counterpart, designated as $(VPGFG)_6$, were synthesized separately using solid-phase peptide synthesis methods. These modules were then conjugated by the copper-catalyzed azide-alkyne cycloaddition "click" reaction. The CLP has a melting temperature at ~50 °C, which ensures that the block polypeptide can form stable triple helices at the physiological conditions. Interestingly, the conjugate CLP–ELP formed well-defined nanovesicles even at 4 °C, which is significantly below the T_t of the ELP block. This could be explained as the CLP–ELP conjugate first assembled through the collagen-like domain to form a triple helix, which induced the localization of ELP domains and thus had a significant effect on reducing the T_t of the conjugated ELP (Fig. 12a). Therefore, ELP domains collapsed even at 4 °C to form a vesicle wall, where CLPs are exposed at the interior and exterior surfaces (Fig. 12a). TEM image confirmed the hypothesis that the 22-nm-thick vesicle wall could be the result of two CLP helices (9.1 nm each) and the approximate length of the collapsed ELP (3.4 nm). The vesicle is stable over a wide range of temperatures, even at those higher than the CLP melting point (50 °C); however, some helices unfolded into single chains. At 80 °C, the CLP chains completely disassembled, leading to vesicle disassociation (Fig. 12a). While ELP-based block copolymers often form micelles but rarely vesicles,[87] this work suggested a facile approach for ELPs for constructing a high-payload carrier for drug delivery. The follow-up work from the same group has demonstrated drug loading and delivery of them into collagen-containing matrices, given that the surface-exposed single-chain CLP can recognize and interact with collagen-rich substrates.[138] Model drugs were demonstrated to be encapsulated within the hollow structure of the vesicle and can be gradually released over a three-week period. Rapid release by thermal triggers can be induced at the unfolding temperature of the CLP domain. Biocompatiblity with different cell lines, such as fibroblasts, chronocytes, and macrophages, was also examined, the results of which implied that the material is biocompatible and does not induce inflammation. If the system could be tuned to a lower temperature near physiological conditions, it would be beneficial to use for controlled release *in vivo* using hyperthermia treatment.

In addition to CLPs, ELPs were very recently conjugated to resilin-like polypeptides (RLPs), designated as repeats of the basic motif QYPSPGRG. Although RLPs, as the name indicates, have ubiquitous properties resembling those of native resilin (i.e., superior resilience),[139,140] the focus of the RLP–ELP conjugates, described in the work of Weitzhandler *et al.*, was on the differences in their hydrophobicity/hydrophilicity to construct amphiphilic block structures.[141] While ELPs exhibit LCST self-assembly as previously discussed, RLPs exhibit upper critical solution temperature (UCST) self-assembly.[142] Therefore, the RLP sequence in a RLP–ELP conjugate is expected to act as a hydrophobic domain, while the ELP sequence, with A as the guest residue and at a sufficient length, is expected to act as a hydrophilic domain. Obviously, as an amphiphilic block copolymer, RLP–ELP would most likely assemble into a micelle-like structure with the hydrophobic core from RLP. There was a threshold in RLP lengths required for micelle formation that was independent of the corona ELP lengths. Interestingly, RLP–ELP transited from micellar to cylindrical morphologies when the hydrophilic weight fractions were changed. The transition took place when the length of RLP increased or the guest A residues were replaced with V residues, which decreased the relative hydrophilicity of ELP. Cylindrical morphologies from ELP systems are rare and thus would further expand the use of ELP-based systems. For example, reports have shown that elongated flexible protein-based nanostructures might be more beneficial in escaping phagocytosis and in penetrating into and extravasating from tissues than their spherical counterparts.[143,144]

Another report described the fabrication of a chimeric polypeptide that incorporates CLP, RLP, and ELP into one polypeptide chain.[145] Herein, RLP, ELP, and CLP sequences were designated as PKG-$(PGG)_5$-K-$(PAG)_5$-PKG, $(LGGVG)_3$-K$(LGGVG)_4$, and $(SDTYGAPGGGNGGRP)_4$, and in the order of N-terminal, central, and C-terminal regions, respectively. K residues were

Please do not adjust margins

Please do not adjust margins

introduced for chemical crosslinking if desired. Nanofibers were formed by heating the block polypeptide suspension in water at 37 °C. The fiber formation could be driven by the self-assembly of the ELP domain, which has a glycine-rich domain-inspired pattern $(XGGZG)_n$. The formation of β-sheets was detected by CD spectra; however, in the presence of RLP and CLP, the resulting nanofibers had features that are different from those previously shown for LGGVG repeating motifs. A network of flexible, aligned fibers were observed, and they were different from the

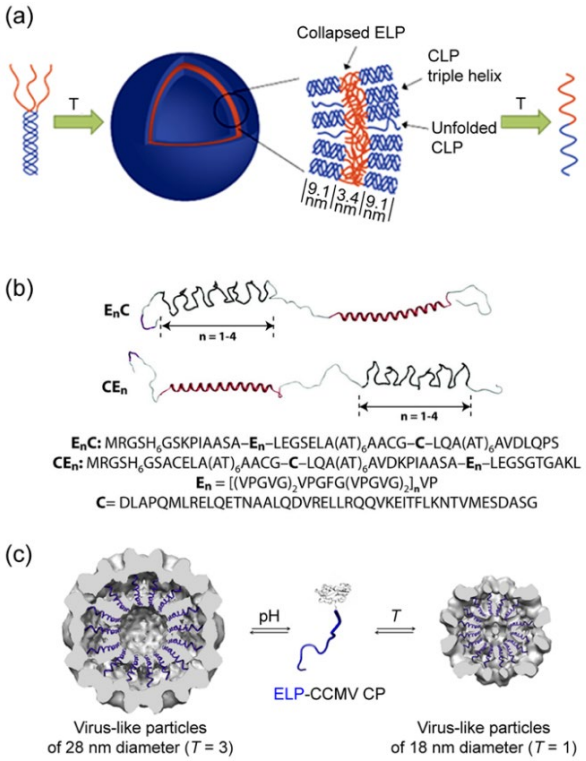

Fig. 12 (a) Schematic of the self-assembly of CLP–ELP conjugate to form a vesicle with a collapsed elastin layer and the interior and exterior surface-exposed collagen triple helix layer. The vesicle disassembles into monomers caused by the disassembly of the triple helix with increasing temperature. Reproduced and adapted with permission from ref. 137. Copyright 2015, American Chemical Society. (b) Illustration of the E_nC and CE_n protein block polymers and their sequences where n represents the number of E repeats. Reproduced and adapted with permission from ref. 150. Copyright 2011, American Chemical Society. (c) Temperature- and pH-induced self-assembly of the ELP-CCMV coat protein fusion, resulting in two types of nanoparticles: one similar to the wild-type CCMV (T = 3 symmetry) and the other with a smaller diameter (T = 1 symmetry). Reproduced and adapted with permission from ref. 152. Copyright 2012, American Chemical Society.

twisted, beaded fibrils from ELPs alone. RLPs alone typically form complex morphologies from particles to rod-like structures.[146,147] CLPs assembled into highly ordered networks of fibers with the periodic D-band at 67 nm.[132] The Young's modulus of the obtained fibers, measured by AFM, was within a range of 0.1–3 MPa, which suggested the effects from highly elastic materials, such as elastin and resilin. Although the role of each domain was not clearly shown, the work provided a proof-of-concept for introducing various self-assembling domains into one polypeptide chain. Further work on evaluating the functions of collagen (e.g., cell adhesion and/or proliferation driven by the collagen domains) or on the macroscale mechanical properties of hydrogel-based chimeric polymers would be of great interest.

5-3. ELP-coiled-coil conjugates

A coiled-coil is another self-associating protein motif in which two or more α-helices assemble to form a supercoil. Montclare *et al.* developed protein block polymers composed of an ELP domain (E) and the coiled-coil derived from cartilage oligomeric matrix protein (C).[148-151] These two different self-assembling domains were fused together in the order of either EC or CE. Although they were similar in their compositions, the EC and CE diblocks exhibited distinct temperature-dependent conformational changes.[148] Only the EC assembled into a hydrogel, while CE became a viscous solution under the identical conditions.[149] The libraries of E_nC and CE_n (n = 1–4) with different E lengths were constructed to further highlight the differences in these subsets (Fig. 12b).[150] All protein polymers (0.2 mg.mL^{-1}) exhibited incrementally elevated T_t values in phosphate buffered saline (PBS) as the E domain was shortened; however, interestingly, the range of the T_t change for the E_nC series was narrower (9.5 °C) than that of the CE_n series (32 °C). The E_nC members (15 mg.mL^{-1} in PBS) showed viscoelastic behavior and assembled into gels above their T_t values. In contrast, the CE_n counterparts remained as a viscous solution at all temperatures tested. The E_nC library could form loose networks through the interactions of the E domain in the β-structured state, which was indicated by CD spectroscopy. Triblock CEC has also been recently constructed.[151] CEC formed a gel, even below its T_t, in which the α-helical C blocks were responsible for network formation. This triblock had the best binding affinity to a small hydrophobic molecule, curcumin, compared to that of the other constructs, such as CE. These works demonstrated that the order of building blocks affects the self-assembly and the resultant physicochemical properties.

5-4. ELP fusion with virus coat protein

The fusion of ELP with a self-assembling coat protein from a virus, such as one from cowpea chlorotic mottle virus (CCMV), is another strategy for creating a hybrid system that exhibits multiple stimuli-induced self-assemblies.[152] CCMV is a 28-nm-icosahedral plant virus comprising 180 coat protein subunits in a T = 3 symmetry. The particle is stable at low pH (~5.0) and disassembles at pH ~7.5.[153] The virion, with a hollow structure, can be used as a protein nanoparticle-based carrier for delivering genetic materials and drugs,[154,155] as well as macromolecules such as enzymes.[156] Combining with an ELP counterpart enabled both pH- and temperature-responsive properties (Fig. 12c).[152] It has been demonstrated that the temperature-driven self-assembly resulted in a nanoparticle with a diameter of 18 nm and a T = 1 symmetry assembled from 60 coat protein (CP)–ELP fusion. The tightly packed

 This journal is © The Royal Society of Chemistry 20xx

Please do not adjust margins

Please do not adjust margins

nanostructures here are the result of the association from the hydrophobic ELP domains after a thermal trigger. On the other hand, pH-driven self-assembly produced a morphology similar to that of the wild-type CCMV (T =3 symmetry). In addition, the presence of different ELP variants, especially those with higher hydrophobicity, could further stabilize CCMV under the physiological conditions.[157] Because the cargos can be protected from proteases, the system could be a promising candidate for *in vivo* studies as drug carriers. Furthermore, the hollow nanoparticle can efficiently load enzymes for use as bionanoreactors.[158]

6. The emerging applications of ELPs

The emerging and exciting research field using ELPs is expanding into more advanced bioengineering, in which ELPs can be used to control functions of a conjugated biomolecule, or as a tool to elucidate biological processes. In this last section, we introduce some of these challenging researches.

Functional enzymes for applications such as biosensors, biofuel synthesis, and biocatalysts, have been increasingly recognized. To efficiently achieve these functions, spatial control over protein density and orientation is important. Synthetic polymers were used to control the self-assembly of the polymer–protein for biofunctional nanostructures.[159,160] Qin *et al.* have constructed an ELP–globular protein (mCherry) conjugation as a model molecule to show that these could achieve the same purpose by self-assembling into highly ordered nanostructures.[161,162] In contrast to the synthetic polymer systems, the globular protein–ELP conjugates can be biosynthesized by a cost-effective process with high yields and excellent monodispersities.[163,164] The phase diagrams of ELP–mCherry fusions were determined to demonstrate the versatility of the conjugate to form various structures, including disordered micellar, hexagonal, oblique, and lamellar nanostructures.[161] When assembling, the ELP domain collapsed and thus allowed the orientation of the conjugated mCherry. The assembled structures were strongly influenced by various factors, such as concentrations, temperatures, ELP hydrophobicity, and ELP charges.[162,165] Formation of lamellar, a well-defined periodic layer structure that could be confirmed by SAXS, was favorable with uncharged hydrophobic ELPs. Meanwhile, charged ELPs were not suitable for highly ordered structures because of electrostatic repulsion. The ELPs that have a balance of negative and positive charge distribution, while not show long-range ordered structures, are highly birefringent at high concentrations.[165] In addition, the effects of the chain arrangement in the ELP–mCherry block structure (e.g., ELP20–mCherry or ELP10–mCherry–ELP10 with or without His-tag) were investigated in detail.[161] These fundamental studies are important for determining the spatial control of functional proteins, such as enzymes or fluorescent proteins, for biocatalysis or optical applications, in which well-arranged, high-density modules and/or orientation are necessary.

Diehl *et al.* used ELP conjugates to control and probe cooperativity in biomotor assemblies.[166] They have engineered a multimotor model system, in which monomeric kinesin-1 motors were anchored to an artificial protein scaffold. ELPs were inserted between basic leucine zipper domains within the scaffold, while the complementary acidic zipper was fused to kinesin-1. Mixing of the scaffold and the acidic zipper-conjugated kinesin-1 allowed the association between them through a coiled-coil formation. This design provided precise control over the spatial and elastic coupling of the motors. The cooperative interactions between monomeric kinesin-1 motors enhanced hydrolysis activity and the gliding velocity of the microtubule; however, these interactions were not influenced by changes in the elastic properties of the scaffold, which were induced by the phase transition of the ELPs. This result suggests that the mechanism by which multimotors are transported is distinct from that driven by unorganized monomeric motors.

The formation of subcellular compartments represented by nuclei and mitochondria is ubiquitous in life. The creation of synthetic compartments in cells is of great interest for engineering cellular behaviors. Ge *et al.* developed a fusion protein consisting of an ELP and green fluorescent protein (GFP) in *E. coli* and plant cells.[167] The ELP-tagged fluorescent protein formed liquid droplets or phase-separated protein-rich microcompartments within the cells, which was indicated by fluorescence recovery after photobleaching experiments. Mackay *et al.* transfected human embryonic kidney HEK-293 cells with the plasmid encoding GFP–ELP, in which GFP was fused to $(VPGVG)_n$ at various chain lengths.[168] The GFP–ELPs expressed in the cells had a diffusion constant similar to that of cytosolic proteins at below their T_t. In contrast, microdomains assembled from GFP–ELPs with a diameter of 0.1–2 μm showed reduced diffusion coefficients above their T_t. The assembly and disassembly of microdomains were rapid processes with the half-lives of 3.8 and 1.0 min, respectively. The temperature-responsive formation of protein microdomains by GFP–ELPs was demonstrated even in the individual cells of zebrafish embryos.[169] This work might aid the studies on developmental biology by allowing for the tunable assembly of functional proteins inside ~~of~~ vertebrate embryos.

The same group also showed ELP coassembly and self-sorting of in cells.[170] Different monoblock ELPs with similar T_t coassembled to form microdomains, while these microdomains self-sorted from the nanoparticles assembled by the ELP diblock amphiphiles (Fig. 13).

ELPs were further fused to a clathrin-light chain (CLC), a protein associated with clathrin-mediated endocytosis.[171] The ELP–CLC reversibly switched off clathrin-mediated endocytosis upon a temperature trigger. This system can be a new platform for the temporal manipulation of trafficking mechanisms in cells.

Li *et al.* reported an intracellular transglutaminase-catalyzed polymerization approach for the efficient synthesis of ELPs and *in situ* construction of topology-controlled nanostructures (Fig. 14).[172] Through a rational design of monomeric peptide sequences, the resultant ELPs exhibited different phase transition behaviors of either the LCST or UCST type. Various topological nanostructures such as nanoparticles and gels, were formed *in situ* in the cytoplasm and exhibited different biofunctions toward retention efficiency and cytotoxicity. In particular, the ELP gels with a volume phase transition at 37 °C

This journal is © The Royal Society of Chemistry 20xx

Please do not adjust margins

Please do not adjust margins

accelerated cell apoptosis, which can be potentially used for drug-free cancer therapy.

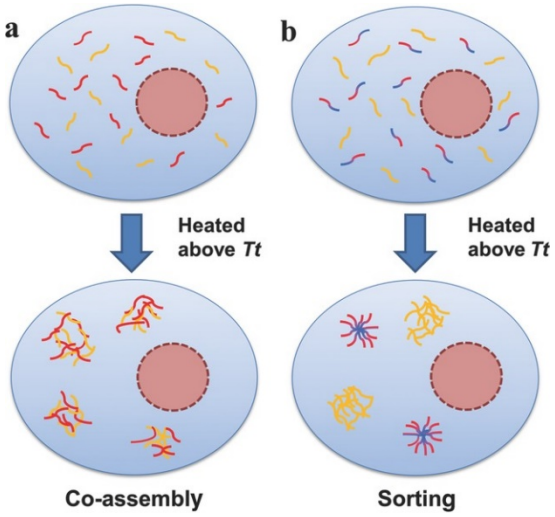

Fig. 13 (a) Two different soluble ELP monoblocks are uniformly distributed in the eukaryotic cytosol at below their T_ts. When induced to phase separation, ELP monoblocks with similar structures coassemble into micron-sized microdomains. (b) Structurally distinct ELP monoblock and diblock copolymers are homogeneously mixed below T_t. After heat-induced transition, the ELP diblocks self-sort into nanoparticles and spatially separate from the microdomains assembled from the ELP monoblocks in the eukaryotic cell model. Reproduced and adapted with permission from ref. 170. Copyright 2013, Wiley-VCH.

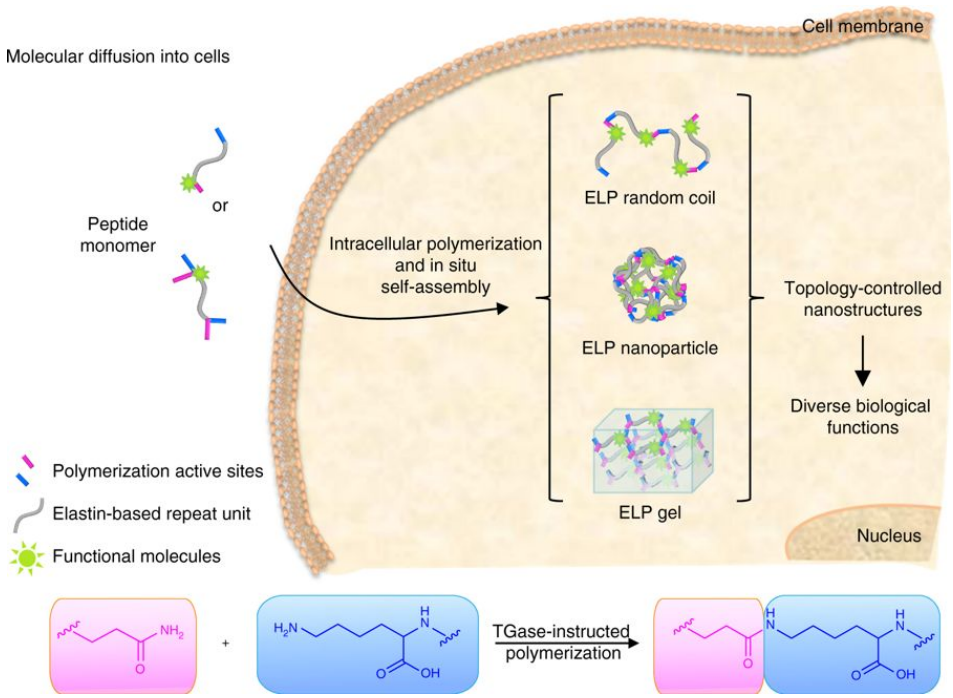

Fig. 14 Schematic illustration of intracellular transglutaminase-catalyzed polymerization and *in situ* controllable construction of nanostructures. The peptide monomer is composed of an elastin-based repeat unit, one-pair or two-pair polymerization active sites, and a functional molecule. Peptide monomers diffuse into cells and are polymerized intracellularly to form topology-controlled nanostructures including one-dimensional elastin-like polypeptide (ELP) random coils, three-dimensional ELP nanoparticles or ELP gels. These structure-differentiated ELP nanostructures exhibited diverse biological functions *in situ*. Reproduced and adapted with permission from ref. 172. Copyright 2017, Nature Publishing Group.

7. Conclusions and Outlook

Inspired by the remarkable elasticity and self-assembling properties of natural elastin, a group of protein polymers called elastin-like polypeptides (ELPs) was created, with the first generation containing the simple $(VPGXG)_n$ repetitive sequences showing LCST behaviors similar to the naturally occurring protein, tropoelastin. From there, thorough investigations on the relationships between the sequence and the phase transition temperature (T_t) helped to establish the general rules for sequence design to precisely control the T_t of ELPs. Meanwhile, another series of tropoelastin-derived $(XGGZG)_n$ repetitive sequence, which exhibits the different and unique self-assembly behavior to form amyloid-like nanofibers,

 This journal is © The Royal Society of Chemistry 20xx

Please do not adjust margins

Please do not adjust margins

was also revealed. These two types of repetitive sequences have become the basic modules for creating ELP-based protein polymers. Advances in synthetic chemistry and genetic engineering has further facilitated the construction of a myriad of ELP-based protein polymers, either in a form of mono- or block ELPs. Not only are ELPs elastic, as in natural elastin, they were also found to have favorable biological characteristics, such as low platelet adhesion and low immunogenicity, which imply their applicability in the biomedical sector. Block polymers consisting of multiple $(VPGXG)_n$-based segments with different T_ts can form micelles, vesicles, or hydrogels derived from their amphiphilicity. The combined use of VPGXG- and VGGVG-based segments gave rise to the formation of flexible nanofibers through the nanoparticle formation and their one-dimensional assembly. These self-assembly systems are promising "smart" drug delivery vehicles or tissue engineering scaffolds because they can be designed to respond to various cues from the surrounding environments, such as temperature, pH, and enzymatic activities. In addition, their mechanical properties and biological functions can be further tuned by crosslinking and modification with functional peptide motifs, respectively. Recently, ELPs have been fused to various self-assembling proteins/peptides derived from silk, collagen, resilin, and coiled-coils. Elaborate self-assembly systems with combined physicochemical properties from different block components can be created, allowing for *de novo* functional materials. For example, synergistic effects were found in the ELP–collagen fusion with an unexpectedly lower T_t compared to that of a single domain ELP because of the localization effect. Hydrogels from silk–ELP could use the rigid β-sheet structures from the silk-like domain and the flexible ELP domain for engineering mechanical properties. Finally, ELP conjugates are beginning to be used as advanced nanobiosystems, including spatiotemporal control of proteins of interest for enhancing protein function or understanding biological machinery, self-sorting materials within cells, and molecular switches for functional proteins. Although it was beyond the scope of this review, the coassembly of ELPs with other molecules could be an exciting direction for creating dynamic self-assembly systems.[173] For example, ELP molecules and peptide amphiphiles were shown to spontaneously coassemble into a closed membrane that can be maintained in a non-equilibrium state for substantial periods of time. The membrane underwent morphogenesis into tubular structures with high spatiotemporal control by mechanical perturbations, which allows for the fabrication of bioactive scaffolds for guiding cell growth.[173]

In summary, with the described excellent controllability of physicochemical properties and unique mechanical/biological characteristics, ELPs are definitely one of the powerful tools for designing ingenious protein molecular devices for nanobioapplications. We hope that this review will stimulate researchers new ideas in incorporating ELPs, the simple yet efficiently designed molecule, in their molecular design strategies for new lines of frontier research.

Conflicts of interest

There are no conflicts to declare.

Acknowledgements

A part of this work was supported by JSPS KAKENHI (16H05911) and JST A-STEP (AS282I011e).

References

1. Y. J. Yang, A. L. Holmberg, B. D. Olsen, *Annu. Rev. Chem. Biomol. Eng.*, 2017, **8**, 549-575.
2. C. Y. Lin, J. C. Liu, *Curr. Opin. Biotechnol.*, 2016, **40**, 56-63.
3. M. Haider, V. Leung, F. Ferrari, J. Crissman, J. Powell, J. Cappello, H. Ghandehari, *Mol. Pharmaceut.*, 2005, **2**, 139-150.
4. A. M. Kushner, Z. Guan, *Angew. Chem. Int. Ed. Engl.*, 2011, **50**, 9026-9057.
5. S. Mondal, M. Varenik, D. N. Bloch, Y. Atsmon-Raz, G. Jacoby, L. Adler-Abramovich, L. J. Shimon, R. Beck, Y. Miller, O. Regev, E. Gazit, *Nat. Commun.*, 2017, **8**, 14018.
6. E. Gazit, *Annu. Rev. Biochem.*, 2018, **87**, 533-553.
7. J. C. Rodriguez-Cabello, F. J. Arias, M. A. Rodrigo, A. Girotti, *Adv. Drug Deliv. Rev.*, 2016, **97**, 85-100.
8. G. C. Yeo, B. Aghaei-Ghareh-Bolagh, E. P. Brackenreg, M. A. Hiob, P. Lee, A. S. Weiss, *Adv. Healthc. Mater.*, 2015, **4**, 2530-2556.
9. E. R. Wright, V. P. Conticello, *Adv. Drug Deliv. Rev.*, 2002, **54**, 1057-1073.
10. S. M. Mithieux, A. S. Weiss, *Adv. Protein Chem.*, 2005, **70**, 437-461.
11. W. F. Daamen, J. H. Veerkamp, J. C. M. van Hest, T. H. van Kuppevelt, *Biomaterials*, 2007, **28**, 4378-4398.
12. C. M. Kielty, M. J. Sherratt, C. A. Shuttleworth, *J. Cell Sci.*, 2002, **115**, 2817-2828.
13. D. Miranda-Nieves, E. L. Chaikof, *ACS Biomater. Sci. Eng.*, 2017, **3**, 694-711.
14. J. Rnjak, S. G. Wise, S. M. Mithieux, A. S. Weiss, *Tissue Eng., Part B*, 2011, **17**, 81-91.
15. D. W. Urry, M. M. Long, B. A. Cox, T. Ohnishi, L. W. Mitchell, M. Jacobs, *Biochim. Biophys. Acta.*, 1974, **371**, 597-602.
16. D. W. Urry, *Angew. Chem. Int. Ed. Engl.*, 1993, **32**, 819-841.
17. A. Pepe, D. Guerra, B. Bochicchio, D. Quaglino, D. Gheduzzi, V. P. Ronchetti, A. M. Tarnburro, *Matrix Biol.*, 2005, **24**, 96-109.
18. A. Pepe, B. Bochiechio, A. M. Tamburro, *Nanomedicine*, 2007, **2**, 203-218.
19. B. Bochicchio, A. Pepe, R. Flarnia, M. Lorusso, A. M. Tamburro, *Biomacromolecules*, 2007, **8**, 3478-3486.
20. A. M. Tamburro, A. Pepe, B. Bochicchio, D. Quaglino, I. P. Ronchetti, *J. Biol. Chem.*, 2005, **280**, 2682-2690.
21. E. E. Fletcher, D. D. Yan, A. A. Kosiba, Y. Zhou, H. F. Shi, *Protein Expres. Purif.*, 2019, **153**, 114-120.
22. A. M. Tamburro, B. Bochicchio, A. Pepe, *Biochemistry*, 2003, **42**, 13347-13362.
23. B. Bochicchio, A. Pepe, *Chirality*, 2011, **23**, 694-702.
24. L. D. Muiznieks, F. W. Keeley, *J. Biol. Chem.*, 2010, **285**, 39779-39789.
25. G. C. Yeo, C. Baldock, A. Tuukkanen, M. Roessle, L. B. Dyksterhuis, S. G. Wise, J. Matthews, S. M. Mithieux, A. S. Weiss, *Proc. Natl. Acad. Sci. U. S. A.*, 2012, **109**, 2878-2883.
26. D. V. Bax, U. R. Rodgers, M. M. M. Bilek, A. S. Weiss, *J. Biol. Chem.*, 2009, **284**, 28616-28623.

Please do not adjust margins

Please do not adjust margins

27. S. G. Wise, G. C. Yeo, M. A. Hiob, J. Rnjak-Kovacina, D. L. Kaplan, M. K. C. Ng, A. S. Weiss, *Acta Biomater.*, 2014, **10**, 1532-1541.
28. S. M. Mithieux, B. Aghaei-Ghareh-Bolagh, L. P. Yan, K. V. Kuppan, Y. W. Wang, F. Garces-Suarez, Z. Li, P. K. Maitz, E. A. Carter, C. Limantoro, W. Chrzanowski, D. Cookson, A. Riboldi-Tunnicliffe, C. Baldock, K. Ohgo, K. K. Kumashiro, G. Edwards, A. S. Weiss, *Adv. Healthc. Mater.*, 2018, **7**.
29. A. C. Rincon, I. T. Molina-Martinez, B. de Las Heras, M. Alonso, C. Bailez, J. C. Rodriguez-Cabello, R. Herrero-Vanrell, *J. Biomed. Mater. Res. A*, 2006, **78a**, 343-351.
30. G. Ciofani, G. G. Genchi, I. Liakos, A. Athanassiou, V. Mattoli, A. Bandiera, *Acta Biomater.*, 2013, **9**, 5111-5121.
31. C. H. Luan, R. D. Harris, K. U. Prasad, D. W. Urry, *Biopolymers*, 1990, **29**, 1699-1706.
32. B. Li, V. Daggett, *Biopolymers*, 2003, **68**, 121-129.
33. D. W. Urry, *J. Phys. Chem. B*, 1997, **101**, 11007-11028.
34. N. K. Li, F. G. Quiroz, C. K. Hall, A. Chilkoti, Y. G. Yingling, *Biomacromolecules*, 2014, **15**, 3522-3530.
35. S. Roberts, M. Dzuricky, A. Chilkoti, *FEBS Lett.*, 2015, **589**, 2477-2486.
36. M. A. Stuart, W. T. Huck, J. Genzer, M. Muller, C. Ober, M. Stamm, G. B. Sukhorukov, I. Szleifer, V. V. Tsukruk, M. Urban, F. Winnik, S. Zauscher, I. Luzinov, S. Minko, *Nat. Mater.*, 2010, **9**, 101-113.
37. A. P. Blum, J. K. Kammeyer, A. M. Rush, C. E. Callmann, M. E. Hahn, N. C. Gianneschi, *J. Am. Chem. Soc.*, 2015, **137**, 2140-2154.
38. D. E. Meyer, A. Chilkoti, *Biomacromolecules*, 2004, **5**, 846-851.
39. A. Ribeiro, F. J. Arias, J. Reguera, M. Alonso, J. C. Rodriguez-Cabello, *Biophys. J.*, 2009, **97**, 312-320.
40. F. Aladini, C. Araman, C. F. Becker, *J. Pept. Sci.*, 2016, **22**, 334-342.
41. J. R. McDaniel, D. C. Radford, A. Chilkoti, *Biomacromolecules*, 2013, **14**, 2866-2872.
42. A. Girotti, J. Reguera, F. J. Arias, M. Alonso, A. M. Testera, J. C. Rodriguez-Cabello, *Macromolecules*, 2004, **37**, 3396-3400.
43. Y. H. Cho, Y. J. Zhang, T. Christensen, L. B. Sagle, A. Chilkoti, P. S. Cremer, *J. Phys. Chem. B*, 2008, **112**, 13765-13771.
44. A. Thapa, W. Han, R. H. Simons, A. Chilkoti, E. Y. Chi, G. P. Lopez, *Biopolymers*, 2013, **99**, 55-62.
45. H. Reiersen, A. R. Rees, *Protein Eng.*, 2000, **13**, 739-743.
46. T. Christensen, W. Hassouneh, K. Trabbic-Carlson, A. Chilkoti, *Biomacromolecules*, 2013, **14**, 1514-1519.
47. J. A. Mackay, D. J. Callahan, K. N. Fitzgerald, A. Chilkoti, *Biomacromolecules*, 2010, **11**, 2873-2879.
48. R. Herrero-Vanrell, A. C. Rincon, M. Alonso, V. Reboto, I. T. Molina-Martinez, J. C. Rodriguez-Cabello, *J. Control. Release*, 2005, **102**, 113-122.
49. M. Alonso, V. Reboto, L. Guiscardo, V. Mate, J. C. Rodriguez-Cabello, *Macromolecules*, 2001, **34**, 8072-8077.
50. D. J. Callahan, W. E. Liu, X. H. Li, M. R. Dreher, W. Hassouneh, M. Kim, P. Marszalek, A. Chilkoti, *Nano Lett.*, 2012, **12**, 2165-2170.
51. J. A. MacKay, M. N. Chen, J. R. McDaniel, W. G. Liu, A. J. Simnick, A. Chilkoti, *Nat. Mater.*, 2009, **8**, 993-999.
52. J. Hu, G. Wang, X. Liu, W. Gao, *Adv. Mater.*, 2015, **27**, 7320-7324.
53. K. Z. Huang, N. J. Duan, C. M. Zhang, R. Mo, Z. C. Hua, *Sci. Rep.*, 2017, **7**.
54. H. Betre, L. A. Setton, D. E. Meyer, A. Chilkoti, *Biomacromolecules*, 2002, **3**, 910-916.
55. W. B. Jeon, B. H. Park, J. Wei, R. W. Park, *J. Biomed. Mater. Res. A*, 2011, **97a**, 152-157.
56. A. Fernandez-Colino, F. J. Arias, M. Alonso, J. C. Rodriguez-Cabello, *Biomacromolecules*, 2015, **16**, 3389-3398.
57. J. C. Rodriguez-Cabello, I. G. de Torre, A. Ibanez-Fonseca, M. Alonso, *Adv. Drug Deliver. Rev.*, 2018, **129**, 118-133.
58. M. K. McHale, L. A. Setton, A. Chilkoti, *Tissue Eng.*, 2005, **11**, 1768-1779.
59. N. Annabi, S. M. Mithieux, E. A. Boughton, A. J. Ruys, A. S. Weiss, F. Dehghani, *Biomaterials*, 2009, **30**, 4550-4557.
60. I. G. de Torre, M. Santos, L. Quintanilla, A. Testera, M. Alonso, J. C. R. Cabello, *Acta Biomater.*, 2014, **10**, 2495-2505.
61. A. M. Testera, A. Girotti, I. G. de Torre, L. Quintanilla, M. Santos, M. Alonso, J. C. Rodriguez-Cabello, *J. Mater. Sci. Mater. Med.,*, 2015, **26**, 105.
62. M. J. Glassman, R. K. Avery, A. Khademhosseini, B. D. Olsen, *Biomacromolecules*, 2016, **17**, 415-426.
63. Y. N. Zhang, R. K. Avery, Q. Vallmajo-Martin, A. Assmann, A. Vegh, A. Memic, B. D. Olsen, N. Annabi, A. Khademhosseini, *Adv. Funct. Mater.*, 2015, **25**, 4814-4826.
64. M. S. Tjin, A. W. C. Chua, D. R. Ma, S. T. Lee, E. Fong, *Macromol. Biosci.*, 2014, **14**, 1125-1134.
65. S. M. Staubli, G. Cerino, I. G. De Torre, M. Alonso, D. Oertli, F. Eckstein, K. Glatz, J. C. R. Cabello, A. Marsano, *Biomaterials*, 2017, **135**, 30-41.
66. D. L. Nettles, A. Chilkoti, L. A. Setton, *Adv. Drug Deliv. Rev.*, 2010, **62**, 1479-1485.
67. W. Kim, E. L. Chaikof, *Adv. Drug Deliv. Rev.*, 2010, **62**, 1468-1478.
68. R. Flamia, P. A. Zhdan, M. Martino, J. E. Castle, A. M. Tamburro, *Biomacromolecules*, 2004, **5**, 1511-1518.
69. L. L. del Mercato, G. Maruccio, P. P. Pompa, B. Bochicchio, A. M. Tamburro, R. Cingolani, R. Rinaldi, *Biomacromolecules*, 2008, **9**, 796-803.
70. M. Martino, A. Coviello, A. M. Tamburro, *Int. J. Biol. Macromol.*, 2000, **27**, 59-64.
71. A. M. Salvi, P. Moscarelli, G. Satriano, B. Bochicchio, J. E. Castle, *Biopolymers*, 2011, **95**, 702-721.
72. A. M. Salvi, P. Moscarelli, B. Bochicchio, G. Lanza, J. E. Castle, *Biopolymers*, 2013, **99**, 292-313.
73. E. Chatani, H. Yagi, H. Naiki, Y. Goto, *J Biol Chem*, 2012, **287**, 22827-22837.
74. P. Moscarelli, F. Boraldi, B. Bochicchio, A. Pepe, A. M. Salvi, D. Quaglino, *Matrix Biol.*, 2014, **36**, 15-27.
75. B. Bochicchio, A. Pepe, M. Crudele, N. Belloy, S. Baud, M. Dauchez, *Soft Matter*, 2015, **11**, 3385-3395.
76. V. Secchi, S. Franchi, M. Fioramonti, G. Polzonetti, G. Iucci, B. Bochicchio, C. Battocchio, *Mater. Sci. Eng., C*, 2017, **77**, 927-934.
77. F. Boraldi, P. Moscarelli, B. Bochicchio, A. Pepe, A. M. Salvi, D. Quaglino, *Sci. Rep.*, 2018, **8**, 3115.
78. J. Cappello, J. Crissman, M. Dorman, M. Mikolajczak, G. Textor, M. Marquet, F. Ferrari, *Biotechnol. Prog.*, 1990, **6**, 198-202.
79. M. J. Fournier, H. S. Creel, M. T. Krejchi, T. L. Mason, D. A. Tirrell, K. P. Mcgrath, E. D. T. Atkins, *J. Bioact. Compat. Polym.*, 1991, **6**, 326-338.
80. J. R. McDaniel, J. A. Mackay, F. G. Quiroz, A. Chilkoti, *Biomacromolecules*, 2010, **11**, 944-952.
81. D. E. Meyer, A. Chilkoti, *Biomacromolecules*, 2002, **3**, 357-367.
82. T. A. T. Lee, A. Cooper, R. P. Apkarian, V. P. Conticello, *Adv. Mater.*, 2000, **12**, 1105-1110.
83. M. H. Misbah, L. Quintanilla, M. Alonso, J. C. Rodrguez-Cabello, *Polymer*, 2015, **81**, 37-44.
84. M. R. Dreher, A. J. Simnick, K. Fischer, R. J. Smith, A. Patel, M. Schmidt, A. Chilkoti, *J. Am. Chem. Soc.*, 2008, **130**, 687-694.
85. W. Hassouneh, E. B. Zhulina, A. Chilkoti, M. Rubinstein, *Macromolecules*, 2015, **48**, 4183-4195.
86. R. E. Sallach, M. Wei, N. Biswas, V. P. Conticello, S. Lecommandoux, R. A. Dluhy, E. L. Chaikof, *J. Am. Chem. Soc.*, 2006, **128**, 12014-12019.

 This journal is © The Royal Society of Chemistry 20xx

Please do not adjust margins

Please do not adjust margins

87. L. Martin, E. Castro, A. Ribeiro, M. Alonso, J. C. Rodriguez-Cabello, *Biomacromolecules*, 2012, **13**, 293-298.
88. D. W. Urry, T. M. Parker, M. C. Reid, D. C. Gowda, *J. Bioact. Compat. Polym.*, 1991, **6**, 263-282.
89. M. Shah, P. Y. Hsueh, G. Sun, H. Y. Chang, S. M. Janib, J. A. MacKay, *Protein Sci.*, 2012, **21**, 743-750.
90. H. Kobayashi, R. Watanabe, P. L. Choyke, *Theranostics*, 2013, **4**, 81-89.
91. W. Kim, J. Thevenot, E. Ibarboure, S. Lecommandoux, E. L. Chaikof, *Angew. Chem. Int. Ed.*, 2010, **49**, 4257-4260.
92. W. Y. Kim, J. T. Xiao, E. L. Chaikof, *Langmuir*, 2011, **27**, 14329-14334.
93. P. Shi, S. Aluri, Y. A. Lin, M. Shah, M. Edman, J. Dhandhukia, H. G. Cui, J. A. MacKay, *J. Control. Release*, 2013, **171**, 330-338.
94. J. Pille, S. A. M. van Lith, J. C. M. van Hest, W. P. J. Leenders, *Biomacromolecules*, 2017, **18**, 1302-1310.
95. S. V. Devi, R. W. Park, *Cancer Res.*, 2013, **73**, LB-95.
96. A. S. C. Soon, M. H. Smith, E. S. Herman, L. A. Lyon, T. H. Barker, *Adv. Healthc. Mater.*, 2013, **2**, 1045-1055.
97. A. J. Simnick, M. Amiram, W. G. Liu, G. Hanna, M. W. Dewhirst, C. D. Kontos, A. Chilkoti, *J. Control. Release*, 2011, **155**, 144-151.
98. G. Y. Sun, P. Y. Hsueh, S. M. Janib, S. Hamm-Alvarez, J. A. MacKay, *J. Control. Release*, 2011, **155**, 218-226.
99. S. R. MacEwan, A. Chilkoti, *Nano Lett.*, 2014, **14**, 2058-2064.
100. D. H. T. Le, R. Hanamura, D. H. Pham, M. Kato, D. A. Tirrell, T. Okubo, A. Sugawara-Narutaki, *Biomacromolecules*, 2013, **14**, 1028-1034.
101. D. H. T. Le, Y. Tsutsui, A. Sugawara-Narutaki, H. Yukawa, Y. Baba, C. Ohtsuki, *J. Biomed. Mater. Res. A*, 2017, **105**, 2475-2484.
102. D. H. T. Le, T. Okubo, A. Sugawara-Narutaki, *Biopolymers*, 2015, **103**, 175-185.
103. D. H. T. Le, R. Kawakami, Y. Teraoka, T. Okubo, A. Sugawara-Narutaki, *Chem. Lett.*, 2015, **44**, 530-532.
104. T. T. H. Anh, M. Xing, D. H. T. Le, A. Sugawara-Narutaki, E. Fong, *Nanomedicine*, 2013, **8**, 567-575.
105. E. R. Wright, R. A. McMillan, A. Cooper, R. P. Apkarian, V. P. Conticello, *Adv. Funct. Mater.*, 2002, **12**, 149-154.
106. K. Nagapudi, W. T. Brinkman, B. S. Thomas, J. O. Park, M. Srinivasarao, E. Wright, V. P. Conticello, E. L. Chaikof, *Biomaterials*, 2005, **26**, 4695-4706.
107. X. Y. Wu, R. Sallach, C. A. Haller, J. A. Caves, K. Nagapudi, V. P. Conticello, M. E. Levenston, E. L. Chaikof, *Biomacromolecules*, 2005, **6**, 3037-3044.
108. R. E. Sallach, W. X. Cui, F. Balderrama, A. W. Martinez, J. Wen, C. A. Haller, J. V. Taylor, E. R. Wright, R. C. Long, E. L. Chaikof, *Biomaterials*, 2010, **31**, 779-791.
109. S. Aluri, M. K. Pastuszka, A. S. Moses, J. A. MacKay, *Biomacromolecules*, 2012, **13**, 2645-2654.
110. M. B. van Eldijk, F. C. Smits, N. Vermue, M. F. Debets, S. Schoffelen, J. C. van Hest, *Biomacromolecules*, 2014, **15**, 2751-2759.
111. D. Mozhdehi, K. M. Luginbuhl, J. R. Simon, M. Dzuricky, R. Berger, H. S. Varol, F. C. Huang, K. L. Buehne, N. R. Mayne, I. Weitzhandler, M. Bonn, S. H. Parekh, A. Chilkoti, *Nat. Chem.*, 2018, **10**, 496-505.
112. D. Mozhdehi, K. M. Luginbuhl, M. Dzuricky , S. A. Costa, S. Xiong, F. C. Huang, M. M. Lewis, S. R. Zelenetz, C. D. Colby, A. Chilkoti, *J. Am. Chem. Soc.*, 2019, **141**, 945-951.
113. J. P. Anderson, J. Cappello, D. C. Martin, *Biopolymers*, 1994, **34**, 1049-1058.
114. S. Z. Lu, X. Q. Wang, Q. Lu, X. H. Zhang, J. A. Kluge, N. Uppal, F. Omenetto, D. L. Kaplan, *Biomacromolecules*, 2010, **11**, 143-150.
115. J. D. van Beek, S. Hess, F. Vollrath, B. H. Meier, *Proc. Natl. Acad. Sci. U. S. A.*, 2002, **99**, 10266-10271.
116. T. Asakura, J. Ashida, T. Yamane, T. Kameda, Y. Nakazawa, K. Ohgo, K. Komatsu, *J. Mol. Biol.*, 2001, **306**, 291-305.
117. X. X. Xia, Z. G. Qian, C. S. Ki, Y. H. Park, D. L. Kaplan, S. Y. Lee, *Proc. Natl. Acad. Sci. U. S. A.*, 2010, **107**, 14059-14063.
118. L. D. Koh, Y. Cheng, C. P. Teng, Y. W. Khin, X. J. Loh, S. Y. Tee, M. Low, E. Y. Ye, H. D. Yu, Y. W. Zhang, M. Y. Han, *Prog. Polym. Sci.*, 2015, **46**, 86-110.
119. Q. Wang, X. X. Xia, W. W. Huang, Y. N. Lin, Q. B. Xu, D. L. Kaplan, *Adv. Funct. Mater.*, 2014, **24**, 4303-4310.
120. X. X. Xia, Q. B. Xu, X. Hu, G. K. Qin, D. L. Kaplan, *Biomacromolecules*, 2011, **12**, 3844-3850.
121. X. X. Xia, M. Wang, Y. A. Lin, Q. B. Xu, D. L. Kaplan, *Biomacromolecules*, 2014, **15**, 908-914.
122. K. J. Isaacson, M. M. Jensen, A. H. Watanabe, B. E. Green, M. A. Correa, J. Cappello, H. Ghandehari, *Macromol. Biosci.*, 2018, **18**, 1700192.
123. M. D. Golinska, T. T. H. Pham, M. W. T. Werten, F. A. de Wolf, M. A. C. Stuart, J. van der Gucht, *Biomacromolecules*, 2013, **14**, 48-55.
124. W. Hwang, B. H. Kim, R. Dandu, J. Cappello, H. Ghandehari, J. Seog, *Langmuir*, 2009, **25**, 12682-12686.
125. Z. Megeed, M. Haider, D. Q. Li, B. W. O'Malley, J. Cappello, H. Ghandehari, *J. Control. Release*, 2004, **94**, 433-445.
126. R. Dandu, A. Von Cresce, R. Briber, P. Dowell, J. Cappello, H. Ghandehari, *Polymer*, 2009, **50**, 366-374.
127. J. A. Gustafson, R. A. Price, K. Greish, J. Cappello, H. Ghandehari, *Mol. Pharmaceut.*, 2010, **7**, 1050-1056.
128. K. Greish, J. Frandsen, S. Scharff, J. Gustafson, J. Cappello, D. Q. Li, B. W. O'Malley, H. Ghandehari, *J. Gene Med.*, 2010, **12**, 572-579.
129. J. A. Gustafson, R. A. Price, J. Frandsen, C. R. Henak, J. Cappello, H. Ghandehari, *Biomacromolecules*, 2013, **14**, 618-625.
130. A. Fernandez-Colino, F. J. Arias, M. Alonso, J. C. Rodriguez-Cabello, *Biomacromolecules*, 2014, **15**, 3781-3793.
131. L. Cen, W. Liu, L. Cui, W. J. Zhang, Y. L. Cao, *Pediatr. Res.*, 2008, **63**, 492-496.
132. M. D. Shoulders, R. T. Raines, *Annu. Rev. Biochem.*, 2009, **78**, 929-958.
133. Y. Shibasaki, S. Hirohara, K. Terada, T. Ando, M. Tanihara, *Biopolymers*, 2011, **96**, 302-315.
134. T. Z. Luo, K. L. Kiick, *Eur. Polym. J.*, 2013, **49**, 2998-3009.
135. M. K. Wlodarczyk-Biegun, M. W. T. Werten, F. A. de Wolf, J. J. J. P. van den Beucken, S. C. G. Leeuwenburgh, M. Kamperman, M. A. C. Stuart, *Acta Biomater.*, 2014, **10**, 3620-3629.
136. K. Strauss, J. Chmielewski, *Curr. Opin. Biotechnol.*, 2017, **46**, 34-41.
137. T. Z. Luo, K. L. Kiick, *J. Am. Chem. Soc.*, 2015, **137**, 15362-15365.
138. T. Z. Luo, M. A. David, L. C. Dunshee, R. A. Scott, M. A. Urello, C. Price, K. L. Kiick, *Biomacromolecules*, 2017, **18**, 2539-2551.
139. R. S. Su, E. E. Gill, Y. Kim, J. C. Liu, *J. Mech. Behav. Biomed. Mater.*, 2018, **91**, 68-75.
140. L. Q. Li, Z. X. Tong, X. Q. Jia, K. L. Kiick, *Soft Matter*, 2013, **9**, 665-673.
141. I. Weitzhandler, M. Dzuricky, I. Hoffmann, F. G. Quiroz, M. Gradzielski, A. Chilkoti, *Biomacromolecules*, 2017, **18**, 2419-2426.
142. F. G. Quiroz, A. Chilkoti, *Nat. Mater.*, 2015, **14**, 1164-1172.
143. S. Shukla, A. L. Ablack, A. M. Wen, K. L. Lee, J. D. Lewis, N. F. Steinmetz, *Mol. Pharmaceut.*, 2013, **10**, 33-42.
144. D. H. T. Le, E. Mendez-Lopez, C. Wang, U. Commandeur, M. A. Aranda, N. F. Steinmetz, *Biomacromolecules*, 2019, **20**, 469–477.

Please do not adjust margins

Please do not adjust margins

145. A. Bracalello, V. Santopietro, M. Vassalli, G. Marletta, R. Del Gaudio, B. Bochicchio, A. Pepe, *Biomacromolecules*, 2011, **12**, 2957-2965.
146. N. K. Dutta, N. R. Choudhury, M. Y. Truong, M. Kim, C. M. Elvin, A. J. Hill, *Biomaterials*, 2009, **30**, 4868-4876.
147. A. M. Tamburro, S. Panariello, V. Santopietro, A. Bracalello, B. Bochicchio, A. Pepe, *Chembiochem*, 2010, **11**, 83-93.
148. J. S. Haghpanah, C. Yuvienco, D. E. Civay, H. Barra, P. J. Baker, S. Khapli, N. Voloshchuk, S. K. Gunasekar, M. Muthukumar, J. K. Montclare, *Chembiochem*, 2009, **10**, 2733-2735.
149. J. S. Haghpanah, C. Yuvienco, E. W. Roth, A. Liang, R. S. Tu, J. K. Montclare, *Mol Biosyst*, 2010, **6**, 1662-1667.
150. M. Dai, J. Haghpanah, N. Singh, E. W. Roth, A. Liang, R. S. Tu, J. K. Montclare, *Biomacromolecules*, 2011, **12**, 4240-4246.
151. A. J. Olsen, P. Katyal, J. S. Haghpanah, M. B. Kubilius, R. P. Li, N. L. Schnabel, S. C. O'Nei, Y. Wang, M. Dai, N. Singh, R. S. Tu, J. K. Montclare, *Biomacromolecules*, 2018, **19**, 1552-1561.
152. M. B. van Eldijk, J. C. Y. Wang, I. J. Minten, C. L. Li, A. Zlotnick, R. J. M. Nolte, J. J. L. M. Cornelissen, J. C. M. van Hest, *J. Am. Chem. Soc.*, 2012, **134**, 18506-18509.
153. L. Lavelle, J. P. Michel, M. Gingery, *J. Virol. Methods*, 2007, **146**, 311-316.
154. M. Comas-Garcia, R. D. Cadena-Nava, A. L. N. Rao, C. M. Knobler, W. M. Gelbart, *J. Virol.*, 2012, **86**, 12271-12282.
155. I. Barwal, R. Kumar, S. Kateriya, A. K. Dinda, S. C. Yadav, *Sci. Rep.*, 2016, **6**, 37096.
156. L. Schoonen, J. C. M. van Hest, *Methods Mol. Biol.*, 2018, **1798**, 69-83.
157. L. Schoonen, R. J. M. Maas, R. J. M. Nolte, J. C. M. van Hest, *Tetrahedron*, 2017, **73**, 4968-4971.
158. L. Schoonen, R. J. M. Nolte, J. C. M. van Hest, *Nanoscale*, 2016, **8**, 14467-14472.
159. C. S. Thomas, L. Z. Xu, B. D. Olsen, *Biomacromolecules*, 2012, **13**, 2781-2792.
160. C. N. Lam, B. D. Olsen, *Soft Matter*, 2013, **9**, 2393-2402.
161. G. K. Qin, M. J. Glassman, C. N. Lam, D. Chang, E. Schaible, A. Hexemer, B. D. Olsen, *Adv. Funct. Mater.*, 2015, **25**, 729-738.
162. G. K. Qin, P. M. Perez, C. E. Mills, B. D. Olsen, *Biomacromolecules*, 2016, **17**, 928-934.
163. A. Yeboah, R. I. Cohen, C. Rabolli, M. L. Yarmush, F. Berthiaume, *Biotechnol. Bioeng.*, 2016, **113**, 1617-1627.
164. D. M. Floss, M. Sack, J. Stadlmann, J. Scheller, E. Stoger, R. Fischer, U. Conrad, *Plant Biotechnol. J.*, 2008, **6**, 424-424.
165. C. E. Mills, Z. Michaud, B. D. Olsen, *Biomacromolecules*, 2018, **19**, 2517-2525.
166. M. R. Diehl, K. C. Zhang, H. J. Lee, D. A. Tirrell, *Science*, 2006, **311**, 1468-1471.
167. X. Ge, A. J. Conley, J. E. Brandle, R. Truant, C. D. M. Filipe, *J. Am. Chem. Soc.*, 2009, **131**, 9094-9099.
168. M. K. Pastuszka, S. M. Janib, I. Weitzhandler, C. T. Okamoto, S. Hamm-Alvarez, J. A. MacKay, *Biomacromolecules*, 2012, **13**, 3439-3444.
169. Z. Li, D. R. Tyrpak, C. L. Lien, J. A. MacKay, *Adv. Biosyst.*, 2018, **2**, 1800112.
170. P. Shi, Y. A. Lin, M. Pastuszka, H. G. Cui, J. A. MacKay, *Adv. Mater.*, 2014, **26**, 449-454.
171. M. K. Pastuszka, C. T. Okamoto, S. F. Hamm-Alvarez, J. A. MacKay, *Adv. Funct. Mater.*, 2014, **24**, 5340-5347.
172. L. L. Li, S. L. Qiao, W. J. Liu, Y. Ma, D. Wan, J. Pan, H. Wang, *Nat. Commun.*, 2017, **8**, 1276.
173. K. E. Inostroza-Brito, E. Collin, O. Siton-Mendelson, K. H. Smith, A. Monge-Marcet, D. S. Ferreira, R. Pérez Rodríguez, M. Alonso, J. C. Rodríguez-Cabello, R. L. Reis, F. Sagués, L. Botto, R. Bitton, H. S. Azevedo, A. Mata, *Nat. Chem.*, 2015, **7**, 897-904.

 This journal is © The Royal Society of Chemistry 20xx

Please do not adjust margins